



POLITECNICO
MILANO 1863

SCUOLA DI INGEGNERIA INDUSTRIALE
E DELL'INFORMAZIONE

Insight into the cycling behaviour of metal anodes for rechargeable batteries, enabled by systematic electrochemical testing, enhanced with mathematical modelling

TESI DI LAUREA MAGISTRALE IN
ENERGY ENGINEERING - INGEGNERIA ENERGETICA

Jacopo Strada, 944676

Advisor:

Prof. Benedetto Bozzini

Co-advisors:

Prof. Elie-Elisee Georges
Paillard

Dott.ssa Elisa Emanuele

Academic year:

2021-2022

Abstract: Symmetrical coin cells represent the preliminary tool for the analysis of battery materials, enabling the study of electrode/electrolyte systems under realistic operating conditions. Rigorous studies of metal-anode shape changes in battery context and upon cycling are rare and especially important to develop reliable and durable implementation of materials. However, the toolbox for the rigorous study of these systems is still wanting. Therefore, the target of this thesis is the investigation of shape-change and passivation issues of metallic anodes under real operating conditions. This study is based on the systematic combination of experimental data of high statistical quality with new studies that have set the aim of describing the profiles of chronopotentiometric transients via models that describe the electrochemical response through electrokinetic, mass-transport and material evolution parameters. This approach is not common in the literature: anodic and cathodic responses are generally studied in isolation, and, on the other hand, when cycling data is considered, quantitative use of electrochemical time series is very rare and only time-to-failure is taken into account. In addition, this thesis studies the behaviour of new electrolyte materials for Zn and Li batteries. Regarding Zn, the key prospective is that of moving from alkaline environments to low-acid aqueous electrolytes. Specifically, we addressed the scantily investigated topic of organic additives for the suppression of dendrite growth, quaternary ammonium salt (QAS). In addition, we investigated Deep Eutectic Solvents (DESs), as a prospective replacement of aqueous solutions, formed by a QAS and a hydrogen-bond donor compounds. With regard to cells with Li electrodes, we considered the traditional LP30 electrolyte as a benchmark, against which we tested a polymeric one and a polymer/IL mixture.

Key-words: simmetrical coin cells, cycling, shape-change, passivation, DES, IL

1. Introduction

Symmetrical coin cells are a very important tool for the analysis of battery materials in context, enabling the study of electrode/electrolyte systems under realistic operating conditions [1, 2]. In particular, the rigorous study of metal-anode shape changes in battery context and upon cycling are rare and especially important to

develop reliable and durable implementation of these materials. However, the toolbox – both conceptual and experimental – for the rigorous study of these systems is still wanting. Therefore, this thesis project aims to develop an experimental, data analysis and modelling platform, enabling: (i) acquisition of accurate electrochemical data; (ii) data processing that can value, in principle, the whole corpora of data collected – including both long-time trends and short-time transients –, instead of just some integral descriptors and (iii) a rational and quantitative understanding, based on transparent physico-chemical modelling. Pioneering studies paving the way to this approach have appeared recently [3]. In any case, a brief contextualization of the measures adopted in this thesis is necessary, in order to understand the different approach we propose. Speaking of EIS measurements, what the articles generally report is the representation of the experimental curves of different series (in terms of electrolyte or electrodes) where they try to describe the differences with the properties of the materials used [4–6]. In other studies, instead, the modelling aspect is preferred: through the electrical analogy, they want to describe the electrochemical behaviour of the EISs through an equivalent electrical circuit (EEC) [7, 8]. However, not all report the results of the fitting and consequently they do not proceed with a quantitative comparison between the various series. This thesis tries to propose a method that combines the two procedures. By observing the shapes of the EISs it is possible give a rational explanation of the different behaviour, justifying them with the properties of the materials previously analyzed with fundamental electrochemical studies. At the same time, through EECs we want to quantify the electrochemical behaviour by verifying that the numerical results are in line with what is highlighted by the preliminary analysis. EIS measurement are not used for *post-mortem* analysis of the cells, *i.e.* [6, 9, 10], in fact, the common idea is to follow a calendar-ageing trend by making EISs after a certain number of cycles. In this thesis, however, we prefer to see if there is any kind of correlation between the aged EIS, the failure mode and the forms of the cycles. Moreover, we want to propose an alternative method for cycles, since in the past, the target was to compare series of cells with different current density and compare the voltage values reached [11–13]. Actually, in recent years some studies have begun to develop models that could describe the trend of the cycles with the behaviour of the anodes during electrodeposition, as [14, 15], thus going deeper and deeper into the chronopotentiometric transients. However, Chen *et al.* [15] does not take into account the global forms of the cycle due to growth and passivation phenomena. For the analysis of the cycles, we were inspired by model proposed in [3] that take into account the multiplicity of phenomena that occur during the charge and discharge phase at the level of the single transients, but also describe the macroscopic behaviour of the measurement.

It is universally recognized today that the future of sustainability depends on Electrochemical Energy Storage Systems (EESs), ranging from rechargeable batteries for electrical/electronic devices and vehicles, as well as for grid storage. The appropriate management of battery materials – both traditional and novel – is an enabling step. Among the plethora of chemistries implemented or investigated, batteries with metal anodes bear promise of high power- and energy-densities, but exhibit several criticalities, essentially owing to shape-change issues. In the context of these technologies, Zn and Li can be regarded as the two most prospective metals: the first one sustainability and intrinsic safety for stationary applications and the latter allowing ultra-high performances for mobile applications. Zn, used as anode for rechargeable alkaline, ZAB, Zn-Ni and ZIB technologies, is both technically and economically attractive, but it still requires in-depth research and development owing to poor reversibility [16]. Zn metal is not as performing as Li (mass density 65.38 g mol^{-1} , volume density 7.14 g cm^{-3} , theoretical gravimetric/volumetric capacity 820 mAh g^{-1} and 5849 mAh cm^{-3} , standard electrochemical redox potential -0.76 V vs. SHE) [17, 18], nevertheless it exhibits a competitive margin with respect to Li in terms of cost, sustainability and safety. A steady background of research on Zn-based batteries can be tracked in the literature of the last two decades [16, 19, 20], onto which a, perhaps not fully justified [21], upheaval of interest for Zn-based rechargeable batteries has been caused by the claim of reversible intercalation of Zn^{2+} in MnO_2 -based cathodes, that seem to have been brought to interesting performance levels [22, 23]. Notwithstanding advancements of cathode studies, limited progress can be found in the research on the anode. The classical issues of metal anodes seem still to be unsorted, in practice [16, 18, 24]. The major challenges such as the formation of zinc dendrites and electrode shape-change are the biggest issues for Zn-based batteries. The most common way to avoid zinc dendrite formation is to control zinc electrodeposition and dissolution with electrolyte with suitable additives enabling a compact and uniform zinc layer [25, 26]. During electrodeposition, the formation of zinc dendrites is pervasive, which leads to the loss of efficiency and capacity of batteries. The continually growing dendrites will finally pierce the separator causing short circuit. Thus, employing effective methods to inhibit the formation and growth of zinc dendrites is fundamental for the practical application of Zn-based batteries [16, 26]. In this way, carbon materials with various structures and morphologies have been widely applied for suppressing the dendrite formation on the Zn surface due to their high structural diversity and convenient fabrication process [27]: the major mechanism of dendrite suppression using carbon is to reduce the energy barrier of Zn nucleation, thus guiding a uniform Zn deposition. Besides, a large energy barrier for Zn nucleation will also cause higher electrochemical impedance, resulting in unsatisfied rate performance of the battery. To guarantee the uniform Zn deposition, a low but constant nucleation energy barrier over the substrate surface is necessary. Also Zn electrode|electrolyte interface shows a dominant effect on the growth mode of Zn. Recently,

tremendous achievements in designing Zn electrode|electrolyte interphase have been acquired to improve the electrochemical performance of Zn batteries [28], however, there is still a long way to fully solve the issues of metal Zn electrode, especially in aqueous electrolyte. The aqueous electrolytes enable better shape control in the cathodic process, though at the cost of enhanced self-discharge [29, 30]. The most commonly proposed aqueous electrolytes are ZnSO₄-solutions, accompanied by additives, like quaternary ammonium salts (QASs): a class on cationic surfactants, that favours control of anode shape changes [31, 32]. Notwithstanding its advantages in the cathodic process, the aqueous environment cannot prevent the formation of passivating films, that is typical of alkaline environment [33, 34]. Some researchers have shown that adding organic co-solvents into aqueous electrolytes can widen the electrochemical stability window [35]. The co-solvent participates in the solvation sheath of cations and strengthens the O–H bond of water, thus, in principle, enabling the suppression of water reactivity. However, this option is neither well understood nor fully developed and this topic warrants, more research efforts. Then, since a common cause of all failure modes is the interaction of Zn and Zn(II) with water, a promising field of study is the development of low water-activity electrolytes. This thesis contributes to this approach, concentrating on deep eutectic solvents (DESs) and their impact on the cycling of Zn anodes. DESs are systems formed from a eutectic mixture of Lewis or Brønsted acids and bases which can contain a variety of anionic and/or cationic species with low lattice energy and hence low melting points [36]. DESs are now widely acknowledged as a new class of ionic liquid (IL), but compared to the latter, the research into DESs is comparatively at its starting point, with the first paper on the subject only published in 2001 [37]. First Abbott *et al.* [38] classify the first-generation eutectic solvents, based on mixtures of QASs with hydrogen bond donors such as amines, acids and alcohols. DESs are classified into three types based on composition:

1. QAS + MCl_x (metal chloride) with M = Zn, Sn, Fe, Al, Ga;
2. QAS + MCl_x·yH₂O (hydrated metal chloride) with M = Cr, Co, Cu, Ni, Fe;
3. QAS + R⁵Z (hydrogen bond donor) with Z = CONH₂, COOH, OH.

There is also a fourth category [39], similar to the third one, but with the replacement of QAS with a hydrated metal halide while still using an organic hydrogen bond donor such as urea. In general, it is possible to say that DESs are commonly defined as systems composed of a mixture of a hydrogen bond acceptor (HBA) and a hydrogen bond donor (HBD). DESs have other advantages over traditional ILs and traditional aqueous electrolyte: firstly, ILs are expensive, and some of them present high toxicity, as well as having poor biodegradability, biocompatibility and sustainability [40, 41]. By contrast, DESs have lower costs and a much-reduced environmental impact. Secondly, the preparation processes of IL and DES is quite different: while DESs are synthesized by simply mixing the two components, generating no waste and requiring no purification steps, the preparation of ILs is far more difficult and expensive. Finally, ILs are composed entirely of ions, that interact through ionic bonds; DESs are the result of complexation between a HBA and a HBD whose interactions, as discussed above, involve mostly hydrogen bonds [36, 42]. In particular, DESs have been reported as novel electrolytes for rechargeable ZIBs. Moreover, water molecules can be incorporated to improve the conductivity, to increase the diffusion coefficient and lower the viscosity of the DES electrolyte without destroying the eutectic nature of DES in a controlled manner [43]. So, in this work we have considered DES with controlled water quantity, that was added by mixing the low-coast hydrated salt Zn(SO₄)·7H₂O. Two DESs were chosen: choline chloride/urea (ChCl/U) and choline chloride/ethylene glycol (ChCl/EG). The reason why these two DESs were chosen, is that ChCl/EG is much less viscous and with higher conductivity at room temperature [44], however ChCl/U is one of the most widespread and promising DES is choline chloride/urea (ChCl/urea), its key pros being low toxicity and stability, also in the presence of water [43]. Furthermore, a series of cells with aqueous electrolyte was used to compare the results. In particular, the electrolyte consists of 2 M ZnSO₄ QAS as an additive: Cetyltrimethylammonium bromide (CTAB). Therefore, what makes this comparison meaningful is the fact that in all electrolytes there is a QAS, even if with different functions, and the presence of water, which can be the electrolyte itself or a component that modifies its conductivity. for impedance and cycle measurements, there are some references [45, 46] however there are not many studies for DES with water, being recent application. Even though holding a share of 35% of the battery market, vis-à-vis a share of 58% for the lead-acid technology [47], Lithium-ion batteries (LIBs) are by far the single most crucial electrochemical storage technology, at the moment. Present-generation rechargeable LIBs use Li-intercalated carbon anodes, exhibiting a relatively low energy density, largely compensated by good cycling stability. In next-generation Li-based batteries, metallic high-energy density Li anodes will progressively replace the carbon-based ones. In fact, Li metal exhibits the lowest mass (6.94 g mol⁻¹) and volume densities (0.534 g cm⁻³) density among metals, the highest theoretical gravimetric/volumetric capacity (3861 mAh g⁻¹ and 2061 mAh cm³) and an extremely low standard electrochemical redox potential (−3.04 V vs. SHE) [17, 18]. Use of Li metal, currently exhibits limited durability upon cycling, owing to phase-formation related issues, such as: dendrite formation, shape changes and passivation, as well as electrolyte decomposition and poorly controllable solid electrolyte interphase (SEI) formation [17, 48, 49], that are the object of active ongoing research. Li dendrite growth has been related to SEI formation and stability [50]. A fragile SEI, due to different effects for which also the Li⁺ diffusion in the electrolyte plays a key role, is the first reason of the dendrite growth. The two phenomena interact mutually: a fragile SEI allows for a facile dendrite growth, while the dendrite growth leads to a fragile SEI. Wang *et al.* [50] analyzed and described

deeply the interconnection between SEI stability and rate of dendrite growth, and concluded that the dendrite formation is strictly connected with Li^+ diffusion mechanism and Li^+ solvation sheath. These phase-formation issues are strongly connected with the choice of the electrolyte, which influences the reactions and transport phenomena at the electrode|electrolyte interface. In particular, requirements for an ideal Li battery electrolyte are an efficient Li^+ transport, the capacity to promote the formation of SEI without limiting ions transport but reducing the dendrites formation, electrochemical stability, safety and sustainability [51]. The most common electrolyte choice is represented by solutions of lithium salts, particularly LiPF_6 , LiTFSI and LiTDI [52], in organic carbonates (ethylene carbonate EC, dimethyl carbonate DMC, ethylmethyl carbonate EMC, propylene carbonate PC and others, often in admixture, essentially aimed at optimal SEI formation) [53]. However, organic carbonate solvents suffer from severe drawbacks: they are thermodynamically unstable vs. Li, they have a low flash point, high flammability and, of course, are prone to leak [54]. Several alternative solvents have been proposed for Li-ions, among which ILs. ILs are molecular salts liquid below 100 °C often based on ammonium, phosphonium, (benz)imidazolium, pyridinium, piperidinium cations with long alkyl chains, combined with anions (*e.g.* BF_4^- , PF_6^- , and especially TFSI) [55, 56]. They have acquired great popularity on account of many advantages, including low volatility and flammability, tuneable polarity, wide chemical and thermal stability in liquid form, and tuneable functional properties, including viscosity and conductivity. From the electrochemical perspective, they are also attractive since they act as both solvent and electrolyte and on account of their good transport properties and wide electrochemical windows; with respect to traditional media they have peculiarities concerning charge transport, viscosity and solvation as well as much higher structural order at the charged electrochemical interphase [56], locally resembling bulk liquid crystal properties, extending at a considerable distance from the electrode surface, and also holding in the presence of significant amounts of water [54]. IL-based lithium battery electrolytes can be obtained dissolving a Li salt in an IL, generally sharing the same anion. It is now recognized that the addition of ionic liquids into polymer-and-salt systems significantly improves the overall performance of lithium-metal electrodes [54, 57]. Apart from the electrochemical performance, a major advantage is the absence of low temperature-flammable compounds. Most of the polymers and ionic liquids researched for battery applications feature high temperature stability and non-flammability upon heat stress. Finally, the use of polymer-based electrolytes offers the possibility to produce thin-film batteries without an additional separator, which is an advantage in terms of energy density. For the present study, we selected PEGDME as polymer electrolyte, which was used in many applications to enhance the ionic conductivity with a good electrochemical stability [58–60], with 1-butyl-1-methylpyrrolidinium bis(trifluoromethanesulfonyl)imide (Pyr14TFSI) IL. Pyr14TFSI was selected because of its high ionic conductivity along with high electrochemical and chemical stability [61], whence it behaves better than FSI-based ionic liquids [62]. Specifically, pyrrolidinium cations show higher stability with respect to reduction and better compatibility at interface with electrodes, because of the absence of acidic protons and double bonds [63]. LiTFSI was chosen and the solute for this solvent, because it has the same anion as the IL. Unfortunately there is not much literature and studies for this duo.

2. Experimental procedure

2.1 Electrolytes preparation:

- 2.1.1 *Deep Eutectic Solvents:* Four different DES electrolytes were used for symmetrical Zn|Zn coin cells: hydrated 0.1 and 0.3 M ZnSO_4 in reline (abbreviated ChU0.1 and ChU0.3), anhydrous 0.3 M ZnSO_4 in reline (abbreviated AChU) and 0.3 M ZnSO_4 in ethaline (abbreviated ChEG). Reline was first prepared by combining urea ($\text{CO}(\text{NH}_2)_2$) (ACS reagent, 100.5%) and choline chloride ($\text{C}_5\text{H}_{14}\text{ClNO}$) (99% Sigma-Aldrich) (2:1 molar ratio) at a temperature of 70 °C for 1 h until a homogeneous colorless solution was obtained. Then, zinc sulphate was added in reline to obtain a 0.1 and 0.3 M ZnSO_4 -ChU DES electrolyte. To eliminate the intrinsic water inside choline chloride, urea and zinc sulphate powders, a pre-drying process was performed by heating these powders separately at 120 °C under a vacuum for 2 days. After the drying process, the chemicals were delivered into an argon-filled glove box for the preparation of anhydrous reline. The latter was then used for the preparation of AChU. Ethaline was prepared with the same procedure of 0.3 M ZnSO_4 reline using ethylene glycol ($\text{C}_2\text{H}_6\text{O}_2$) (reagent plus, $\geq 99\%$ Sigma-Aldrich) instead of urea.
- 2.1.2 *Li cells electrolytes:* For Li cells, electrolytes consist in a first carbonate solution and two polymer-based solutions with an ionic liquid. The first electrolyte is 1 M lithium hexafluorophosphate in ethylene carbonate and dimethyl carbonate (1 M LiPF_6 in EC/DMC, 50/50 in volume ratio) (Sigma-Aldrich), denoted LP30. The second one consists of poly(ethylene glycol) dimethyl (PEGDME-500, Sigma-Aldrich) with lithium bis(trifluoromethanesulfonyl)imide (LiTFSI), EO:Li = 20 in weight ratio. Last electrolyte is PEGDME:Pyr14TFSI: LiTFSI (20:1:1 in molar ratio), where 1-butyl-1-methylpyrrolidinium-bis(trifluoromethylsulfonyl) (99.9%, Solvionic) is the ionic liquid. For the preparation, LiTFSI was dehydrated in vacuum ambient following these steps: 80 °C for 8 h, 100 °C for 36 h and 120 °C for 2 h. Finally, it was delivered into an argon-filled glove box for the

electrolyte preparation.

2.2 Electrode preparation and cell fabrication: The testing cells were fabricated as a symmetric coin cell (CR2032). For Zn cells, electrodes were made by punching a 250 μm thick Zn foil into a 12 mm diameter disks. A 260 μm thick glass microfiber foil was punched into a 19 mm disk and used as the separator. Instead, Li cells were fabricated in an argon-filled glove box using Li chips (15 mm diameter, 1 mm thick) as electrodes with the same glass microfiber separator of Zn cells, previously dehydrated at 200 $^{\circ}\text{C}$ for 24 h. For both cells 350 μL of electrolyte as prepared in section 2.1, was added to the cell. The structure of the CR2032 cells is shown in Fig. 1.

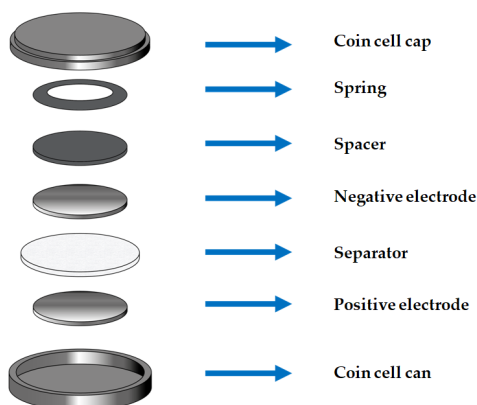


Figure 1: Schematic diagram of CR2032 coin cell configuration.

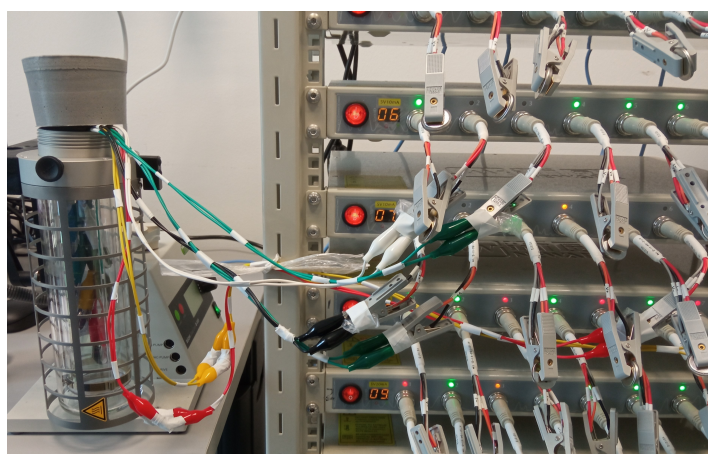
2.3 Electrochemical measurements:

2.3.1 *Electrochemical impedance spectroscopy (EIS):* EIS measurements were performed via VMP-300 biologic potentiostat/galvanostat in the range of 1MHz-100mHz for pristine cells and 1MHz-10mHz for aged cells at OCP.

2.3.2 *Galvanostatic charge-discharge cycle (GCDC):* GCDCs were carried out via NEWARE Battery Testing System (Model: CT-4008T-5V10mA-164). Zn cells were cycled at 0.1, 0.2, 0.5, and 1 mA cm^{-2} for 30 min at each CD and the voltage was limited by setting the cut off to ± 2 V. Li cells were performed at: 0.1 and 10 mA cm^{-2} ($C = 1 \text{ mAh cm}^{-2}$) for LP30 system; 0.05 and 1 mA cm^{-2} ($C = 0.1 \text{ mAh cm}^{-2}$) for PEGDME:Pyr14TFSI systems. Polymer-based cells were performed at 60 $^{\circ}\text{C}$ with BUCHI oven, as shown in Fig. 2.



(a) View of Li polymer-cells inside the BUCHI oven.



(b) Electrical connections.

Figure 2: Cycling systems of Li-polymer cells.

3. Results and discussion

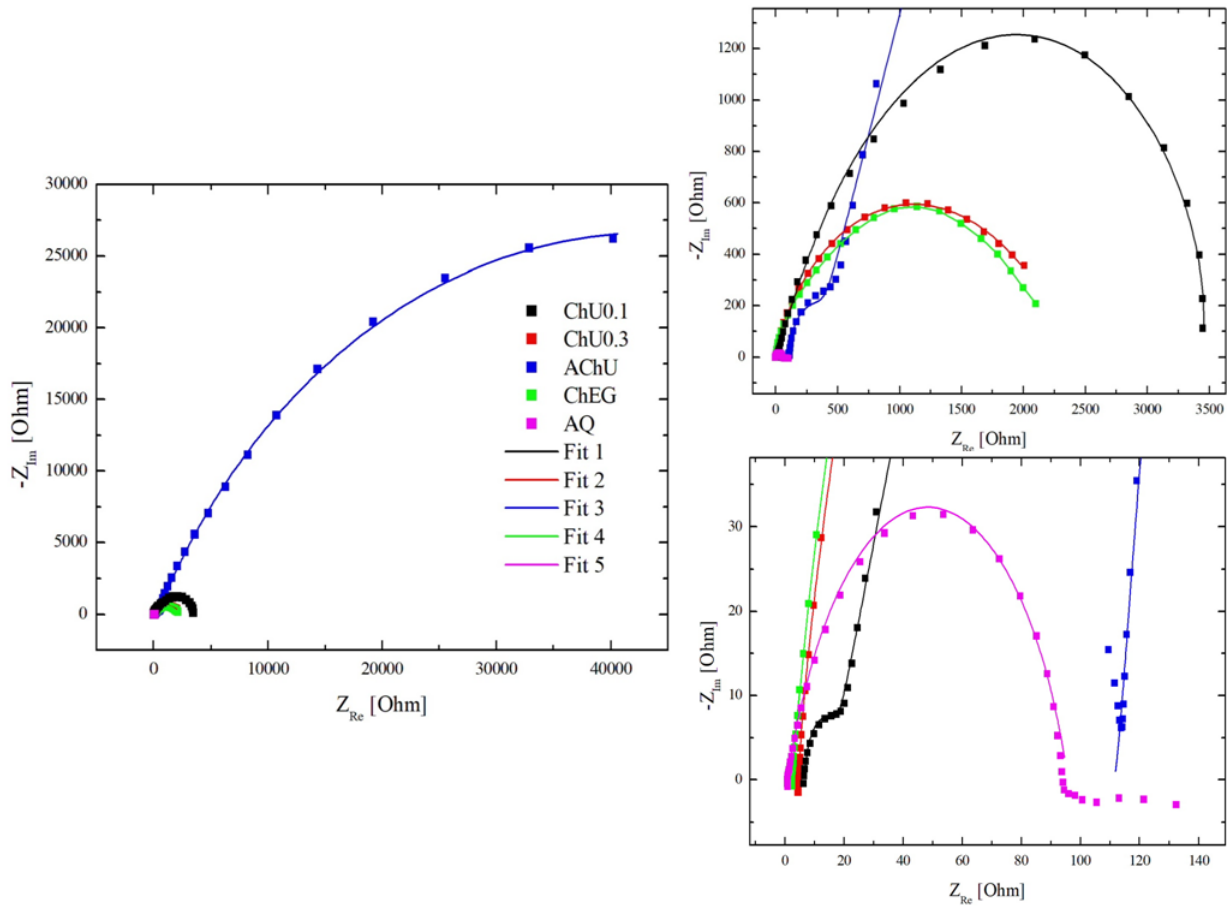
The results were reported based on the technology under observation, then Zn and Li cells are proposed separately. For each, the EIS measurement of the pristine cell, the chronopotentiometric transients and finally the EIS of the post-cycling cells were reported.

3.1. Zinc symmetrical cells with DES-based electrolytes

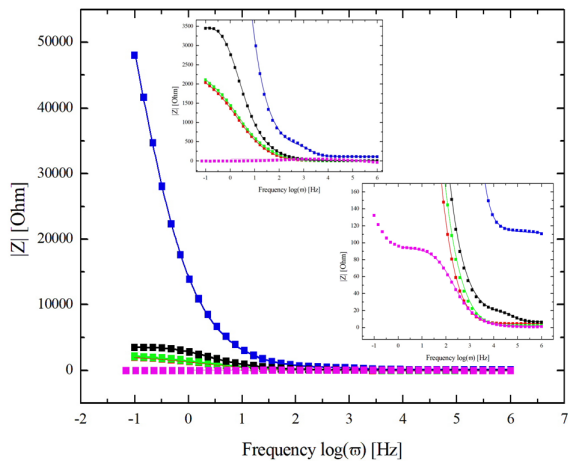
The liquid structure of DES is retained in the presence of water up to 50 vol% while transport properties are improved due to reduced viscosity. Indeed, when excess water is added, such eutectic/H₂O systems would change from a “water-in-eutectic” to an ordinary “aqueous solution” regime [64]. In this work we report the synthesis of hydrated eutectic Zn electrolytes with a precise hydration level, based on a simple formulation, mixing a low-cost hydrated salt Zn(SO₄)·7H₂O with reline and ethaline, as mentioned in Section 2.1.1. In this way, water molecules can be incorporated in the hydrogen bond lattice to improve the conductivity, to increase the diffusion coefficient and lower the viscosity of the DES electrolyte without destroying the eutectic nature of DES in a controlled manner.

3.1.1 EIS of pristine cells

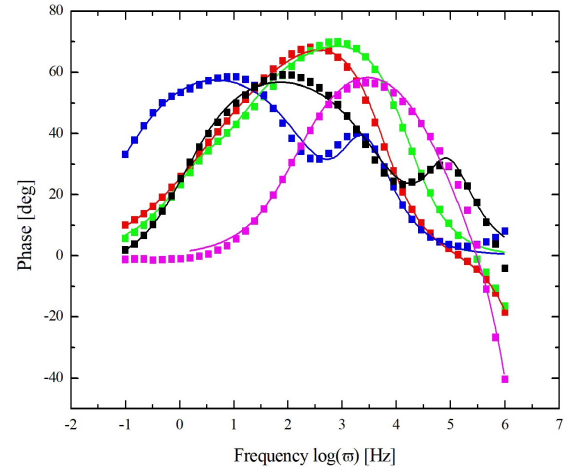
Twelve identical cells for each electrolyte type (ChU0.1, ChU0.3, AChU, ChEG) were assembled to have three replicates for each current density (CD). EIS measurements were carried out in order to verify the correct assembly and test the electrochemical behaviour of the pristine cell. For aqueous series (AQ) series, post-processing work was done with previously assembled cells. Cells of the type described in Section 2.2, were manufactured with a 2 M ZnSO₄ aqueous solution, to which one of six QASs was added: BDMPAC, BPPEI, CTAB, DMDTDAB, PDADMAC and TBAB. The effect of these additives in near-neutral Zn²⁺ aqueous electrolytes has been systematically investigated in previous work in our group [65]. According to our previous work with alkaline [31] and near-neutral electrolytes [65], the additive concentration was 0.1 g L⁻¹ for all QASs except polymeric BPPEI, the concentration of which was 0.01 g L⁻¹. A first analysis was made to compare the aqueous and the DES cases: it was noted that, if the EIS of the DESs are compared to the aqueous with QASs ones, the latter are concentrated in a very small area of Nyquist. For this reason it was decided to take a single characteristic curve to represent the aqueous behaviour with respect to DESs. The choice fell on the series with additive CTAB, due to the structural similarity with ChCl. Observing also the other cases separately, the impedances obtained are similar in shape and size, so it is legitimate to represent the five cases with a single characteristic curve (Fig. 3). The experimental EIS spectra were fitted with the equivalent electrical circuit (EEC) models reported in Fig. 4; a MATLAB script was used for the fitting via Non-linear least squares (NLLS).



(a) Nyquist plot of Zn electrolytes.



(b) Bode magnitude plot of Zn electrolytes.



(c) Bode phase plot of Zn electrolytes.

Figure 3: Pristine EISs of Zn electrolytes.

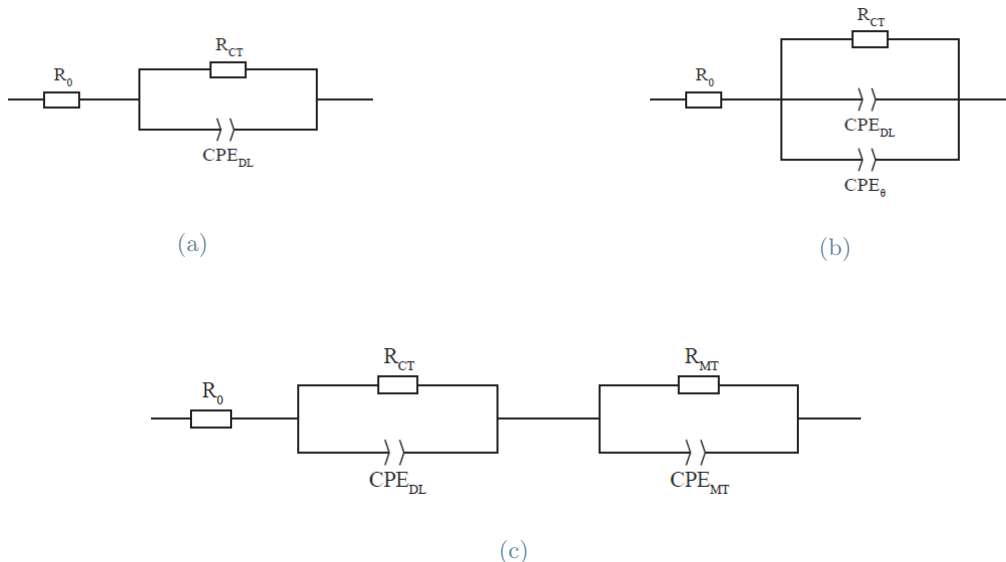


Figure 4: EECs for pristine Zn EISs.

The model 4a represents the typical capacitive-semicircle, used for fitting AQ data. Model 4b, instead, was proposed by De Pauli *et al.* [66] to highlight two different contributions in the electrode|electrolyte interphase, such as an heterogeneous double layer (DL) and the adsorption process on electrode surface. Actually, the parallel of two CPEs was first introduced by Almond and West [67, 68] to analyze the effect of low frequency dispersion in bulk conductivity on the components of electrical impedance, following the empirical equations introduced by Jonscher [69] to represent the imaginary part of the small signal frequency response of dielectric materials and termed “universal dielectric response”. In details, this model takes into account ohmic resistance R_o , the charge-transfer resistance R_{CT} , CPE_{DL} representing the capacity of the DL and CPE_{θ} due to different degree of partial coverage of the electrode surface. The first physical explanation for CPE behaviour is the electrode roughness, meaning that the surface fills between two dimensions (*i.e.* flat surface) and three dimensions (*i.e.* the surface fills three dimensions, branching every-which-way through space, and resembling a porous cube). Another explanation is inhomogeneous reaction rates on a surface; this might be seen at polycrystalline metal surfaces with a distribution of active sites (with varying activation energies) on the surface. A third possible explanation may be varying thickness or composition in the DL. Analyzing our case, a variation of a property along the surface of an electrode can give rise to a constant dispersion over time, which, for an adequate distribution function, can be expressed as a CPE: this would represent the term CPE_{DL} (valid also for model 4a and 4c), expressed also in [66, 70]. Instead, the term CPE_{θ} would have the meaning of a different degree of partial coverage that could derive from two effects: the first effect could be due to the presence of molecular chains differently oriented that modify the conductivity of the DES. Indeed, DES interfaces are inherently more complicated than IL one. Whereas ILs consist of cations and anions only, DESs comprise cations, anions and a molecular components which, for DES:EG and DES:U, has a concentration that is twice that of the parent salt. Chen *et al.* [71] studied a series of DES at HOPG electrode interface as function of potential. Multilayers nanostructures were found, but generally the numbers of layers and the forces between them are less than those reported for ILs. The main difference between the two types of electrolytes is due to the presence of the molecular component, that cannot participate in ionic interactions. The literature report that conveys the most relevant information for our purposes, shows, on the basis of AFM measurements, that, at negative potentials, the Stern layer is enriched in choline with charged groups facing the electrode and alcohol groups facing the bulk liquid while the final measured layer at negative potentials is HBD-rich [71]. A second study found the formation of a potential-dependent compact layer of choline: Vieira *et al.* [72] have studied the adsorbed species on Glassy Carbon (GC) electrode via PM-IRRAS spectroelectrochemistry showing that there is a compact layer made of Ch^+ ions that favors the reduction of hydroxyl group. The choline layer can change the orientation of the charged species (*i.e.* water dipoles). Therefore, there can be differences in the electric field at the interface if the surface is not completely covered by Ch^+ . This means that there are areas of the electrode where the current flows more easily than others. Secondly, CPE_{θ} could represent the effect of the separator: DESs made with urea are usually very viscous and wax-like when the temperature is lower than 25 °C. Given the above, the wettability of the porous separator must be considered: in order to verify a possible effect of the separator, a cell without separator was assembled exactly like the one shown in Fig. 1 (without conical spring) with an O-Ring between the two metal electrodes instead of the separator. The impedance spectrum obtained, however, has the same shape and it remains in the dispersion range of the cells assembled with the separator. It can be

concluded that CPE_{ϑ} is not strongly characterized by the effect of separator on the Zn electrode, but it could be associated with the different orientation of the organic chains, as previously mentioned. Unfortunately, in the literature, articles on the orientation of choline chains in DES are scarce, being recent studies, but it was found that, when H_2O is present in a molar fraction less than 40%, through H-bonds it remains linked to the components of the DES lattice in the form of HBD-water, choline ion-water and chloride ion-water bonds [64]. The reasons given so far imply that ChU0.3 and ChEG can be represented by the same EEC (Fig. 4b). For ChU0.1 and AChU, instead, a different model was used (Fig. 4c). For these two series, a very small R_{CT} is observed, followed by a semicircle that is two orders of magnitude larger, representing mass transport control (R_{MT} and CPE_{MT}): this suggests fast charge-transfer, with mass-transport to the electrode surface ultimately controlling the cell current. Differently, the effect of CPE_{ϑ} was not observed as in the previous cases, because the electrolyte was formed by dehydrated components, eliminating the effect that water has on organic chains, confirming that the presence of water can change the orientation of the chains in the vicinity of DL. Fitting parameters were reported characteristics in terms of mean and standard deviation in Tab. 1.

	ChU0.1	ChU0.3	AChU	ChEG	AQ
R_o [Ω]	5.76 \pm 0.60	4.86 \pm 0.32	120.74 \pm 4.82	2.64 \pm 0.25	0.80 \pm 0.24
R_{CT} [Ω]	11.88 \pm 1.78	1925.97 \pm 487.60	157.53 \pm 76.69	1899.60 \pm 590.50	82.26 \pm 33.58
τ_{DL} [s]	(9.08 \pm 7.89)e ⁻⁶	0.0395 \pm 0.0232	(2.02 \pm 2.07)e ⁻⁵	0.0226 \pm 0.0235	(6.75 \pm 1.60)e ⁻³
α_{DL} [-]	0.931 \pm 0.055	0.892 \pm 0.065	0.883 \pm 0.071	0.952 \pm 0.130	0.735 \pm 0.030
τ_{ϑ} [s]	-	0.386 \pm 0.176	-	0.204 \pm 0.098	-
α_{ϑ} [-]	-	0.412 \pm 0.062	-	0.592 \pm 0.104	-
R_{MT} [Ω]	(3.75 \pm 0.42)e ³	-	(96.18 \pm 31.46)e ³	-	-
τ_{MT} [s]	0.159 \pm 0.022	-	1.744 \pm 0.518	-	-
α_{MT} [-]	0.738 \pm 0.018	-	0.658 \pm 0.039	-	-

Table 1: Fitting parameters of pristine Zn EISs in terms of $\mu \pm \sigma$.

Dwelling on R_o , it varies considerably (AQ<ChEG<ChU0.3<ChU0.1<AChU). AQ is necessarily the lowest since the electrolyte is formed by the Zn salt in water and a limited amount of additive, which therefore makes the electrolyte not very viscous and dense, increasing conductivity. Taking into account DESs cases, the reason for these differences can be found in the physical properties of DES itself: in ChEG the HBD (EG), is liquid and this favours the formation of a less viscous DES. In [36] the relationship between viscosity and conductivity is studied, highlighting how there is a good linear correlation between the molar conductivity and the fluidity (reciprocal of viscosity). Unlike ChEG, ChU0.1 and ChU0.3 are produced by mixing two solid components, creating a more viscous and less conductive substance. The high viscosity is mainly due to the presence of hydrogen bond and Van Der Waals interactions that limit the mobility of ions, as well as to the large ion size and small void volume. Viscosity can affect electrochemical processes; therefore, the development of low-viscosity DESs is highly desirable. The addition of suitable co-solvents, *e.g.* IL/DES-based, can be one promising route [73]. The difference in R_o values between ChU0.1 and ChU0.3 was justified thank to Abbott *et al.* [74] who have studied Zn reduction both in ChCl:U and ChCl:EG, showing that Zn reduction is favourable if concentration of Zn salt is higher than 10^{-4} M, but increasing metal concentration up to 0.3 M leads to a significant reduction in viscosity, with a 65% fall, corresponding to an increase in conductivity: 1200 μ S at 0.1 M and 1600 μ S at 0.3 M, at 25 °C. AChU is the limit case since it has a completely different system: to observe the effect that water has in the system, AChU was produced exactly like ChU0.3 but the components were dried in order to eliminate water content totally (as described in Section 2.1.1). The result of the EIS reflect what was expected: the removal of the water made the DES even more dense and viscous, increasing R_o by two orders of magnitude compared to the other two cases. The diffusion coefficients increases, in general, as the amount of water in the system is increased [64]. Observing R_{CT} between ChU0.3 and ChEG similar results highlight how the two systems have very similar activity, although one is more viscous than the other; it also suggests that the movement of Zn^{2+} ions sees substantially the same resistance. The result obtained is what was expected since the H-donor changes between the two systems but it is not involved in Zn^{2+} transport. In case of ChU0.1 and AChU, however, R_{CT} decreases substantially with respect to ChU0.3 and ChEG. Once again, the reason is found in the absence of water: DES have a high solubility ability for metal salts, metal oxides and hydroxides and at the same time the formation of non-soluble oxide and/or hydroxide is not present. Abbott *et al.* have studied the ion speciation in both ChCl:U and ChCl:EG using EXAFS pointing out that

in both DESs $[\text{ZnCl}_4]^{2-}$ is the dominant species [74]. The chlorinated structure is highly stable and difficult to reduce. The insertion of H_2O has an effect on the ions transport, given the presence of H-bonds within the DESs and the possibility to create more complex solvation spheres around Zn^{2+} , as shown in [75]. However, in electroplating processes the type and concentration of the metal are critical in order to control the morphology and coating rate of the metal deposited. For these reasons knowing the coordination chemistry and the metal complex formed between the Lewis acids of the metal and the Lewis base of the DES is a key factor [74].

3.1.2 GCD cycles

Chronopotentiometric transients were analysed using the model reported by Bozzini *et al.* [3]. As introduced in this paper, the time-dependence of the solutions of parameters can be separated into a slow and a fast regime. The fast regime involves the timescale of a single galvanostatic interval (a half period of the galvanostatic square wave) and controls the shape of each individual chronopotentiometric transient. According to certain model parameters, such as diffusivity D , number density of nuclei and the passivation rate k_{pass} , it is possible to compare the shapes of the transients. Indeed, the proposed model enables to follow the potential transients resulting from the application of a galvanostatic square wave, with a PDE system, coupling the material balance for the electroactive metal species and the potential of the electrolyte phase (by modelling the coin cell in 1D geometry with an adequate approximation). The slow regime, instead, involves the timescale of the whole measurement, that is generally controlled by passivation-induced termination, and defines the evolution of the potential over several galvanostatic periods, defined by the outgrowth rate F_C and the passivation rate k_{pass} . Figures below show the whole cycling obtained for the different CDs and the different electrolytes.

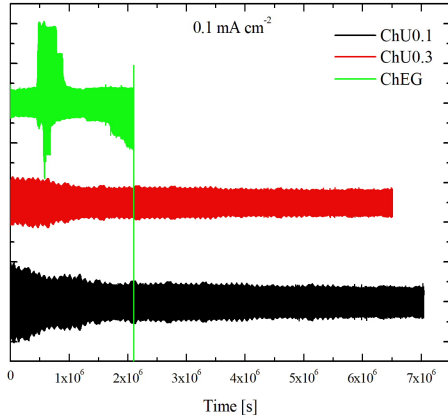


Figure 5: Zn GCD cycles at 0.1 mA cm^{-2} .

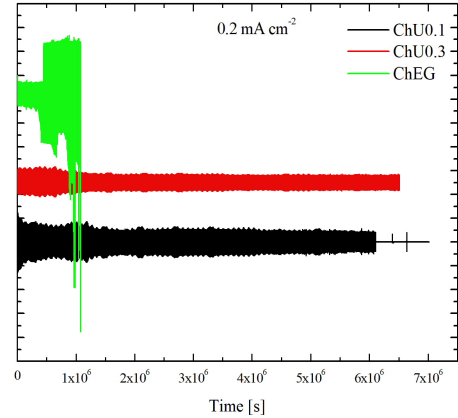


Figure 6: Zn GCD cycles at 0.2 mA cm^{-2} .

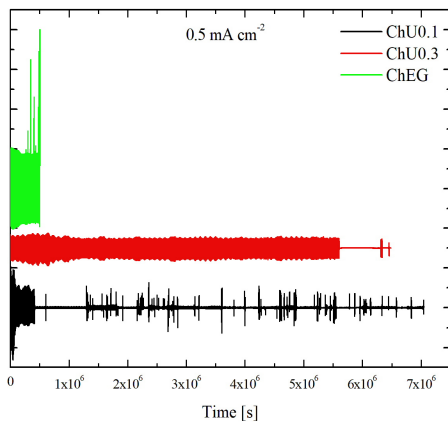


Figure 7: Zn GCD cycles at 0.5 mA cm^{-2} .

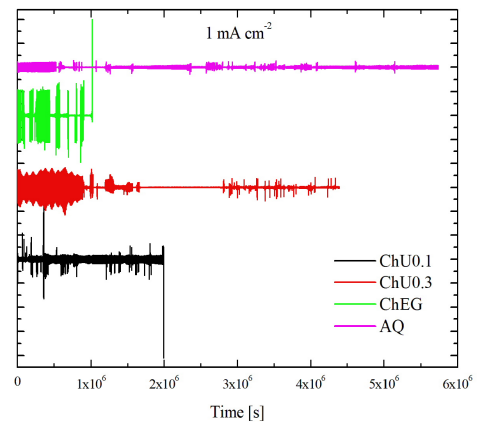


Figure 8: Zn GCD cycles at 1 mA cm^{-2} .

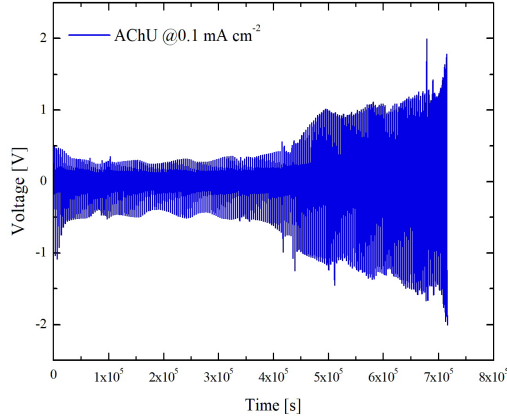


Figure 9: AChU GCD cycle at 0.1 mA cm^{-2} .

The first fact that must be pointed out is the correlation that exists between the amplitudes of the transients immediately after starting the cycling and the impedance measurements made with the pristine cells. With an increase in the current density, the polarization voltages of the cells increase as well, but it is expected that the relationship between the amplitude of the potentials in the initial transients is comparable to the ratio between some EIS parameters in the different cases, regardless of the CD. The chronopotentiometric cycles were sampled second by second, therefore at a frequency of 1 Hz: this prevents the effect of R_o (visible at mH) from being observed directly and quantitatively, however it is possible to express the effect that the impedance has inside the cycles, in terms of $R_o + R_{CT} + R_{MT}$. In fact, observing the initial transients, between ChU0.1 and ChU0.3 a factor of 2 is noted between the potential values for each CD; this is in line with the relationship between $R_o + R_{CT}$. If ChU0.3 and ChEG are compared, the same behaviour in the initial transients is found, since pristine EISs are almost superimposable: this is observed at the currents 0.1 and 0.2 mA cm^{-2} , where the ChEG transients have a slightly lower potential, justified by the lower R_o , however at 0.5 and 1 mA cm^{-2} the ChEG transients undergo a considerable increase, suggesting a certain instability of the EG system at high CDs. At 1 mA cm^{-2} it is possible to compare the AQ system with the other series, since the available data are start with that CD: the measurement of the transients is in line with EIS, especially if these measurements are combined with those of the DESs, which exhibit a notable increase in both transients and impedances. Finally, AChU represents a separate case given that mass transport is the phenomenon that can be observed mainly in EIS; the ability to compare transients becomes, therefore, more complicated due to the high resistance. In conclusion to this first analysis, it can be stated that the relationship that exists between the pristine EISs ($AQ < ChEG < ChU0.3 < ChU0.1 < AChU$) is also found within the initial transients of the cycles, with some exceptions: for high CDs, which make some electrolytes less stable, and in borderline cases such as AChU where the comparison is distorted by the notable presence of mass transport effects.

The analysis can now proceed by grading the systems according to the duration of their life and the termination mode. Excluding AChU, urea-based systems are observed to live the longest: for ChU0.3 (red in Fig. 5, 6, 7 and 8), all cells cycled at 0.1 and 0.2 mA cm^{-2} ($\pm 70 \text{ mV}$ recorded) were still running after 75 days, while those at 0.5 and 1 mA cm^{-2} ($\pm 120 \text{ mV}$ and $\pm 300 \text{ mV}$ respectively) are terminated by short circuit, after 58 ± 7 and 7 ± 4 days respectively (time between the start and the first short circuit). For these two cases it is noted that the chronopotentiometric transients remain stable from the beginning till the end of the test: within two irregular charge-discharge periods (2 h) the cell short-circuits. Comparing with the ChU0.1 (black in Fig. 5, 6, 7 and 8) series, a lengthening of the period in which the cell has a regular behaviour is observed. In fact in ChU0.1 the short circuit occurs at 33 ± 29 and 3 ± 2 days at 0.2 and 0.5 mA cm^{-2} , respectively. Similarly to what happens for ChU0.3, also for ChU0.1 the shape of the transients remains regular and stable up to the vicinity of the short circuit, which occurs after a couple of irregular cycles. At 1 mA cm^{-2} cycles are characterized by square transients of $\pm 50 \text{ mV}$ from the beginning, suggesting a tendency to passivate which however is recovered very well with a fast corrosion during each transient. The fact that for the systems just analyzed, the chronopotentiometric transient remain regular until death cell failure implies a reversible plating/stripping process, as suggested by [3], which makes U-based systems very interesting in view of stable cycling. Thus, none of the cells fails by passivation, that is the dominating failure mode for Zn aqueous cells, even if they exhibit smaller HER and less passivation effect compared with alkaline Zn batteries [76, 77]. The reason lies in the fact that in DES, the small percentage of water has very low activity because of its coordination function, when water enters in the lattice through hydrogen bonds [64, 73]. Indeed due to the bipolar nature, water molecule can act either

like HBD or HBA. Specifically, when water is present in a small amount ($w_{\text{H}_2\text{O}} < 5\%$ or molar fraction less than 30%), it is absorbed in the molecular matrix of DES by forming H-bonds with the ions and HBDs. Zhekenov *et al.* [64] observed a similar behaviour for different DESs in terms of number of hydrogen bonds between the pairs which include water: HBD-water, choline ion-water and chloride ion-water. All of these increase with increasing water in the system. The HBD-water demonstrates the most significant change with high number of hydrogen bonds as water is added into the system, which also reflects high solubility of the components in water. Furthermore, the other components pairs such as HBD-choline ion, HBD-chloride ion and HBD-HBD, have a descending trend with addition of water for all of the DESs. A decrease in these interactions reflects HBDs preference to form hydrogen bonds with water, owing to its high polarity, over other species present in the system. Moreover, looking more closely into the slow regime, for all CDs a peak/depression alternation is observed which according to [3] would suggest an outgrowth/stripping process. However, it is observed how these peaks/depressions have seasonal trend with a period of 1 day linked to the cyclic variation of the ambient temperature: this has been demonstrated with a dedicated experiment in a climatic chamber at fixed temperature (25 °C), that shows a constant potential shape.

Moving on to ChEG (green in Fig. 5, 6, 7 and 8), the typical termination mode is by passivation, visible for 0.1, 0.2 and 0.5 mA cm⁻² after 32±7, 21±15 and 4±1 days respectively. For the last case, at 1 mA cm⁻², a short circuit is reached in 16±12 hours after that cells try to restart the cycling but with some success. In fact, all the three replicates exhibit an alternation between short circuit and chronopotentiometric transient (after the first regular ones) lasting about 22±9 cycles. Finally, after 13±3 days cells reach the cut-off voltage. For 0.1 and 0.2 mA cm⁻² transient amplitude goes from ±70 mV up to ±400 mV, instead for 0.5 and 1 mA cm⁻² transient goes to ±500 mV from starting. Moreover, from the macroscopic point of view it is observed that the EG-based system is subjected to sudden changes in potential which however have very long periods, contrary to what happens to U-based system. In these periods both the transient amplitude and the shape of the transients change.

In the borderline case AChU (Fig. 9), the higher resistance prevents the cells from cycling, if not at very low currents, but in the case at 0.1 mA cm⁻² there is a gradual overpotential growth which after 9±2 days reaches the cut-off voltage. Instead, at 0.2, 0.5 and 1 mA cm⁻² the cells reach 2 V immediately after starting, a value too high for symmetrical cells. These measurements demonstrate the effect of water within the DES; indeed, according to [73], the controlled addition of water inside the DES tunes the conductivity of the electrolyte itself. Comparing GCDC of AU and the others, it is clear how the conductivity, and thus the ohmic resistance of the electrolyte, plays a fundamental role in creating a functioning cell.

Finally, AQ (pink in figures above) is considered. As can be seen from the measurements at 1 mA cm⁻², the cycles do not undergo alterations from outgrowth/passivation of the metal on the surfaces. The cells have a regular shape for 3±2 days (±70 mV), after that there are 19±13 irregular intermediate cycles that separate the regular transients from the short circuit. This confirms what is found in literature: in aqueous electrolyte dendrites formation is a significant problem, causing electrode shape-changes, eventually leading to short circuit [31]. In our case, the intermediate irregular cycles represent the formation of dendrites that cause transient short-circuit conditions. In all the replicates, however, the cells tend to resume the regular behaviour after a period at short circuit, in any case, the regular behaviour periods are relatively brief, and short-circuit conditions tend to occur periodically. It is important to note that Zn metal deposited from DESs are reported to tendentially exhibit compact microcrystalline structure, in contrast to Zn deposited from aqueous electrolytes which tends to have a dendritic structure in the absence of strong additives [31].

To conclude the macroscopic analysis of the cycles, therefore from the point of view of the slow regime, thanks to the model presented in [3] the outgrowth and passivation rates can be obtained. As can be seen from GCDC and from what has been stated so far, ChU0.1 and ChU0.3 do not incur in passivation phenomena. Differently, there is an initial period in which outgrowth of the active electrode surface is observed, where the electrode surface area grows up to ca. 400 cycles regardless of the applied current. To conclude the analysis on U-based systems, AChU exhibits, in common with the other two series, an initial decrease in the potential profile and finally a very fast growth due to the high resistance of the cell which gradually increases. The EG-based electrolyte does not show any phenomenon of initial outgrowth, however it has step-profiles but which have F_C equal to zero inside them. Contrary to the other cases, there is an increase in potential due to passivation, so k_{pass} can be calculated. The overall AQ profile can be assimilated to a flat shape which therefore does not show either outgrowth or passivation.

	ChU0.1	ChU0.3	AChU	ChEG	AQ
F_C	1–450 cycles: $3.1e^{-7}$	1–400 cycles: $3.6e^{-7}$	1–30 cycles: $7e^{-6}$	0	0
k_{pass}	0	0	$4.14e^{-6}$	$4e^{-5}$	0

Table 2: Summary table of F_C and k_{pass} values for Zn electrolytes.

If, on the other hand, the fast regime is taken into account (Fig. 10, 11, 12, 13), it is clearly visible that DES-systems have very similar shapes during cycling. A good symmetry of the shape of the anodic and cathodic regime is noted for U-systems. This behaviour suggests a good reversibility between the outgrowth/stripping processes, also visible at 1 mA cm^{-2} for ChU0.3: deposition and dissolution process are highly reversible. For ChEG, chronopotentiometric transients remain regular and symmetric only at low CDs, but for a determined period of time: the starting 54 ± 47 cycles at 0.1 and 0.2 mA cm^{-2} are represented in Fig. 10 and 11 in green. At 0.5 mA cm^{-2} (Fig. 12), instead, shapes are no more symmetric between cathodic and anodic part, suggesting that EG is not stable as U at high current and outgrowth/stripping process is no longer reversible. This is valid also at 1 mA cm^{-2} (Fig. 13), but after the first short-circuit, cells resume the measurement by recording regular transients but with a different shape: they pass from a simplified arc-shape to a double peak one. Comparing instead ChU0.3 and AChU, the second one has a similar shape but with a quicker growth due to the presence of mass transport effect. Finally, AQ transients are shown in Fig. 13.

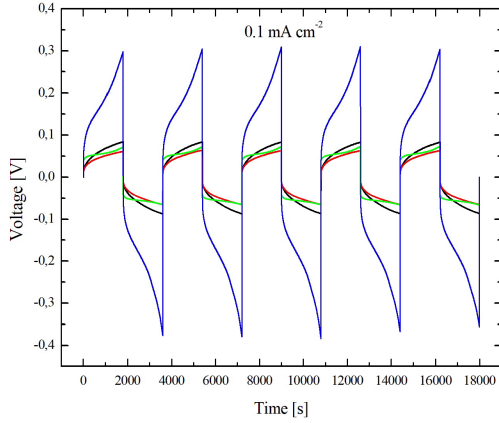


Figure 10: Chronopotentiometric transient of Zn electrolytes at 0.1 mA cm^{-2} .

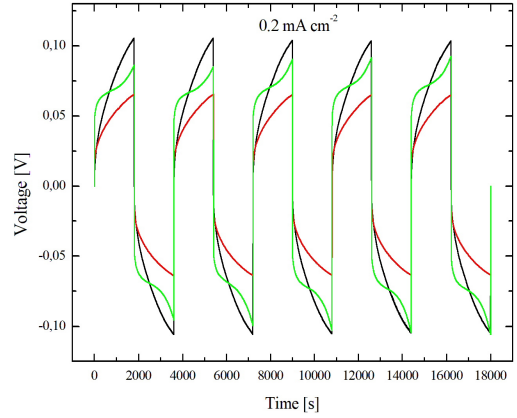


Figure 11: Chronopotentiometric transient of Zn electrolytes at 0.2 mA cm^{-2} .

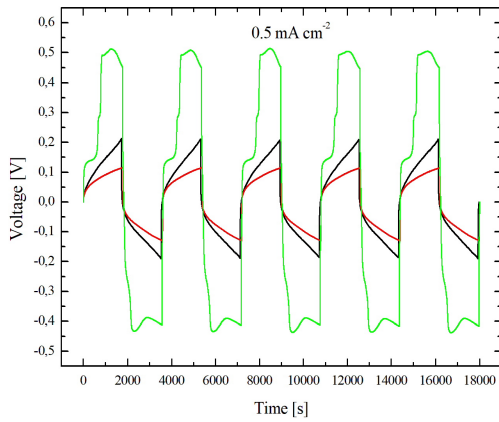


Figure 12: Chronopotentiometric transient of Zn electrolytes at 0.5 mA cm^{-2} .

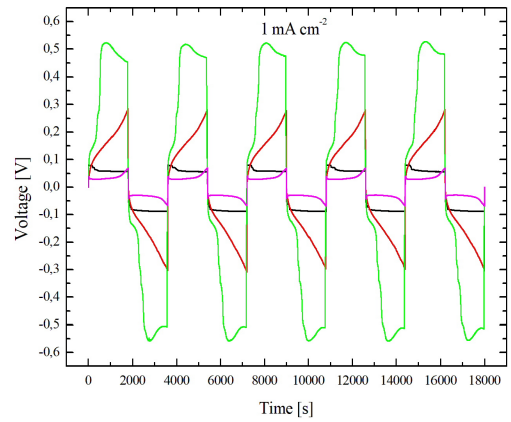


Figure 13: Chronopotentiometric transient of Zn electrolytes at 1 mA cm^{-2} .

In conclusion, most of the transients can be traced back in a more simplified way as an arc-shape transient and, from the comparison between our results and what is reported in [3], it can be concluded that the transient shape

is dominated by the low diffusion coefficient of Zn^{2+} in U-based DESs. This result is in accordance with the fact that DESs have higher viscosity and lower conductivity compared to other ionic liquids [36, 42]. Subsequently, it is observed that the diffusion decreases passing from ChEG to AQ. This is what was expected given that EG has a higher conductivity than U and therefore diffusion is more favoured in the EG-based electrolyte; while between the DESs and the aqueous environment, the diffusion is greater in the latter, where the means is H_2O . Since the additive has the task of controlling shape-change and dendritic growth, it is expected that the r_{\max} value is lower for the AQ case. Based on the shape of the transient and the model reported in [3], this result is confirmed.





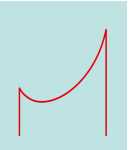
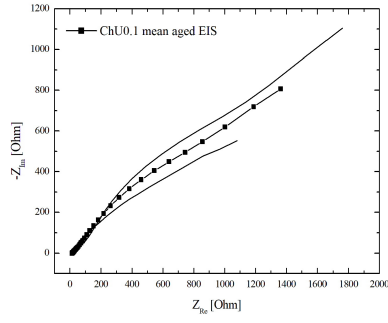
	ChU0.1	ChU0.3	AChU	ChEG	AQ
D [$\text{cm}^2 \text{s}^{-1}$]	$3e^{-7}$	$3e^{-7}$	$3e^{-7}$	$3e^{-6}$	$3e^{-5}$
r_{\max} [mm]	0.05	0.05	0.05	0.037	0.027
k_{pass} [cm s^{-1}]	$3.5e^{-7}$	$3.5e^{-7}$	$3.5e^{-6}$	$3.5e^{-6}$	$1e^{-7}$
shape					

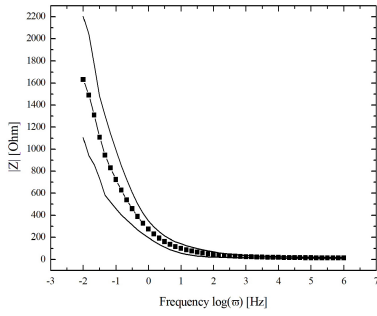
Table 3: Summary table of parameters that describe fast regime.

3.1.3 EIS of aged cells

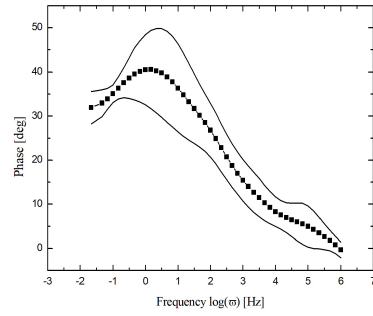
An analysis on failed cells aims to link the last moments of life of the cells themselves during cycling and the termination mode with the impedance spectra measurement. In particular, the idea is to observe if there is an analogy between the shape and size of the EIS with *i.e.* the current with which the cells were run, with failure mode or with pristine EIS. As a preliminary analysis a link was sought between the aged EIS and CDs: it was observed that, for all the cases analyzed, the curves did not have a particular trend, but they were mixed together without being able to distinguish which measures had been cycled to a given CD. The termination method was the second step: also in this case no particular trend was observed for cells that failed due to short circuit or passivation. This may be justified by the fact that the short circuit occurs even if a very small dendrite connects the two electrodes, however, the electrolyte still has activity to be able to dissolve it. This implies that, once an EIS has been measured, it only sees the effect of passivation. The aged EISs for all series are reported in the following figures: it was decided to represent them with their range of dispersion in order to qualitatively visualize the effect of passivation.



(a) Nyquist plot of ChU0.1.

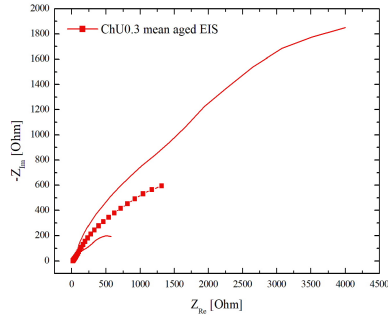


(b) Bode magnitude plot of ChU0.1.

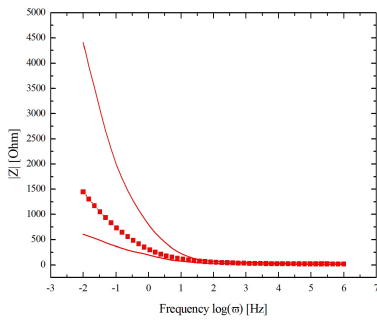


(c) Bode phase plot of ChU0.1.

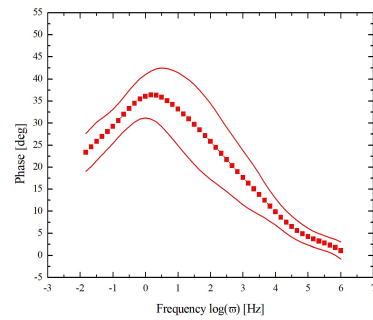
Figure 14: Dispersion of aged ChU0.1 EISs.



(a) Nyquist plot of ChU0.3.

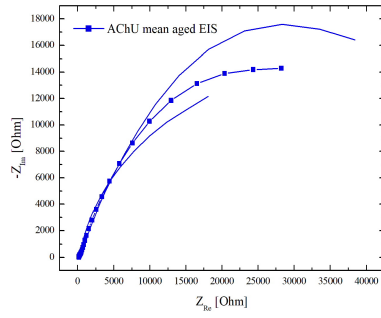


(b) Bode magnitude plot of ChU0.3.

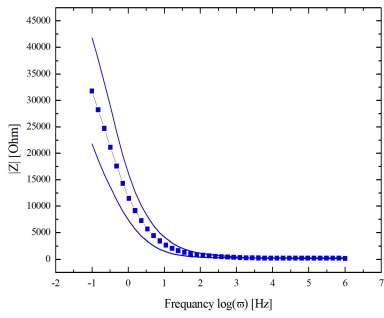


(c) Bode phase plot of ChU0.3.

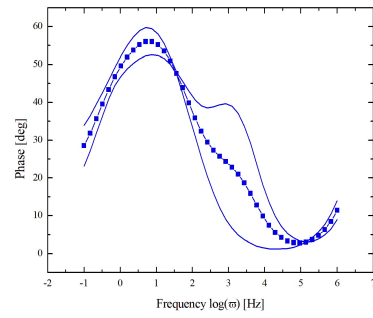
Figure 15: Dispersion of aged ChU0.3 EISs.



(a) Nyquist plot of AChU.

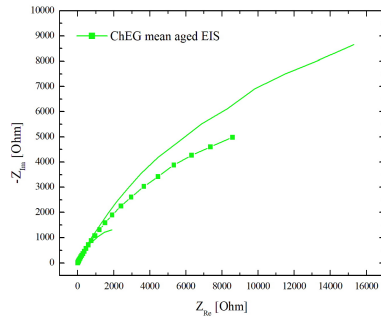


(b) Bode magnitude plot of AChU.

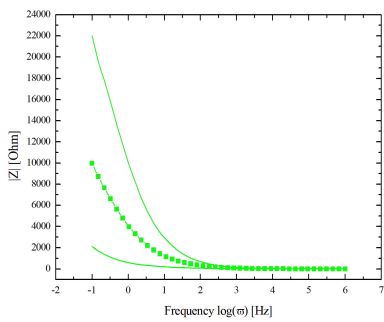


(c) Bode phase plot of AChU.

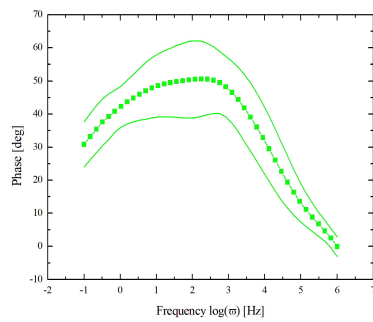
Figure 16: Dispersion of aged AChU EISs.



(a) Nyquist plot of ChEG.

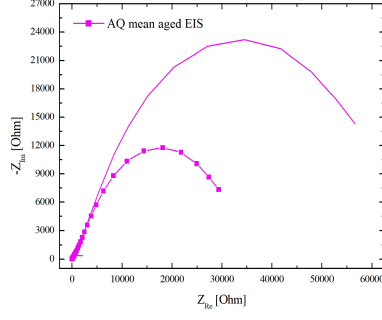


(b) Bode magnitude plot of ChEG.

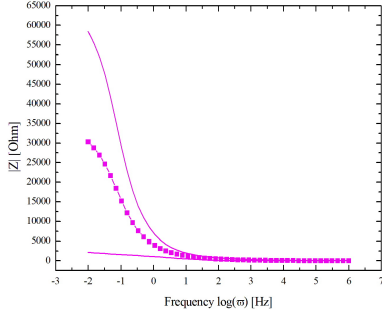


(c) Bode phase plot of ChEG.

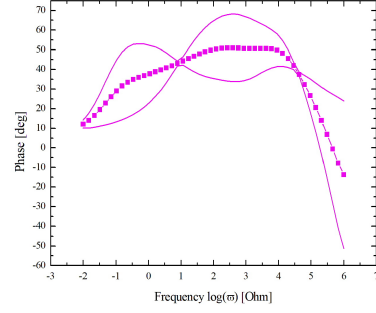
Figure 17: Dispersion of aged ChEG EISs.



(a) Nyquist plot of AQ.



(b) Bode magnitude plot of AQ.



(c) Bode phase plot of AQ.

Figure 18: Dispersion of aged AQ EISs.

The model used for fitting aged EISs is reported in Fig. 19, while in Tab. 4 fitting parameters are reported.

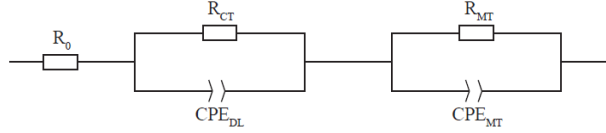


Figure 19: EEC for aged Zn EISs.

	ChU0.1	ChU0.3	AChU	ChEG	AQ
R_o [Ω]	14.96 ± 3.78	17.69 ± 3.68	147.98 ± 38.58	12.47 ± 6.18	5.26 ± 6.68
R_{CT} [Ω]	163.84 ± 262.02	67.09 ± 97.13	178.76 ± 30.03	323.71 ± 340.54	$(1.55 \pm 0.16)e^3$
τ_{DL} [s]	0.331 ± 0.566	$(6.46 \pm 14.83)e^{-2}$	$(1.35 \pm 1.64)e^{-4}$	0.109 ± 0.132	1.283 ± 1.731
α_{DL} [-]	0.561 ± 0.130	0.632 ± 0.171	0.816 ± 0.094	0.476 ± 0.172	0.543 ± 0.049
R_{MT} [Ω]	$(2.64 \pm 2.95)e^3$	$(2.64 \pm 2.69)e^3$	$(10.46 \pm 1.18)e^4$	$(1.51 \pm 1.25)e^4$	$(3.30 \pm 4.51)e^4$
τ_{MT} [s]	$(1.86 \pm 0.91)e^{-3}$	0.366 ± 0.686	2.287 ± 0.768	1.762 ± 1.709	1.315 ± 1.712
α_{MT} [-]	0.645 ± 0.131	0.558 ± 0.084	0.614 ± 0.061	0.489 ± 0.147	0.763 ± 0.019

Table 4: Fitting parameters of aged Zn EISs in terms of $\mu \pm \sigma$.

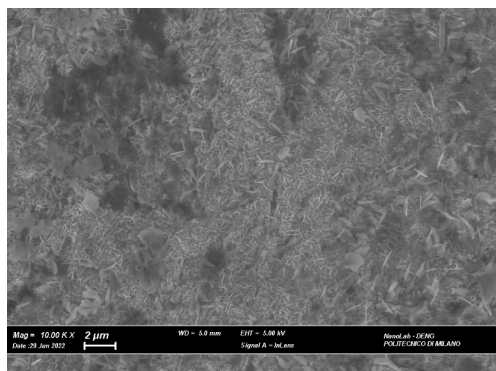
The R_o increases for all cases due to the clogging of the separator, reducing the conductivity of the system (verified once the cells were opened). The conditions of the surface electrodes also change; the interfaces $Zn_1|electrolyte$ and $electrolyte|Zn_2$ are modified due to shape change of the metal surfaces. This causes a variation of the active area that is higher respect to the flat pristine one. Furthermore, we want to underline that the AChU case experience less dispersion and it is the one that differs less from the pristine case, given that these

cells have cycled for a very short time. The opposite case is the AQ one, where a high dispersion is observed due to the phenomenon of passivation in aqueous environment: for all resistance terms the dispersion is very high. Dispersion, on the other hand, is more limited for the other DES-based electrolytes, which however have some differences. ChU0.3 and ChEG had very similar behaviour in terms of pristine EIS, however once cycled, EG is subject to passivation phenomena (as seen in Section 3.1.2) which therefore will have a greater increase in resistances. At the moment, it can be said that passivation in water differs from that in DES, given that, as has already been said previously, it is very important to know the metal complex formed between the Lewis acids of the metal and the Lewis base of the DES. Therefore, this topic needs further clarification which will be the subject of future studies.

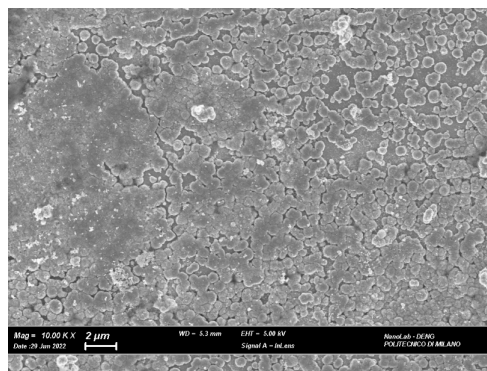
To further characterize the stability and the effects of cycling of Zn in the different systems used, the electrodes were disassembled from the cell and washed with DI water and acetone repeatedly to remove the electrolyte.

3.1.4 SEM analysis of Zn electrodes

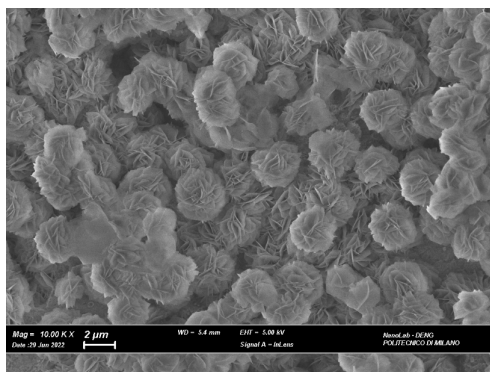
SEM measurements were conducted with the collaboration of Politecnico Nanolab (Energy Department) with special thanks to Doctor Andrea Macrelli. Post-mortem analysis of the structure and morphology of Zn electrodes were investigated using a scanning electron microscope (SEM). Fig. 20. shows the typical morphology of the central area of dismantled Zn anode electrode cycled at 1 mA cm^{-2} in three different electrolytes.



(a) SEM of Zn in AQ electrolyte



(b) SEM of Zn in ChU0.3 electrolyte



(c) SEM of Zn in ChEG electrolyte

Figure 20: SEM measurements

SEM measurements reported above show how the morphology of the Zn metal growths is completely different in three systems. The Zn deposited from the U-based liquid has a “spherical-grain” morphology, with an almost homogeneous crystallites distribution. A very different Zn morphology occurs when aqueous or ChEG systems are used. Indeed, Zn metal grain are covered by thin amorphous plate that can be attributed to the formation of ZnO. In the latter two case it can be said that the overall morphology of the samples is due to the electrodeposited Zn grain (produced during charge process) that are than covered by layers of ZnO (produced in the anodic stripping during the discharge). DESs have a high solubility for metal salts; unusually, this also includes metal oxides and hydroxides, which gives these systems an advantage over aqueous and organic based electrolytes. However, the ZnO solubility in ChU0.3 is much higher than in ChEG. A simple experiment was conducted to prove how the solubility of ZnO can be affected by the two different electrolytes: 10 mg of ZnO were dissolved

in 10 mL of electrolyte and left at 70 °C overnight (Fig. 21). After the stirring and heating process the ChU0.3 DES appears transparent while ChEG looks milky white.

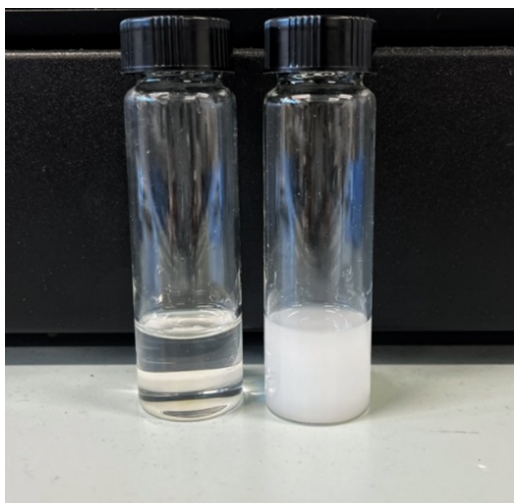


Figure 21: Dissolution of 10 mg ZnO in ChU0.3 (left side) and ChEG (right side).

Zn nuclei grain sizes increase in the order $AQ < ChEG < ChU0.3$, indicating that the aqueous system has the highest nucleation rate constant. Nuclei grain size can be correlated to different physical-chemical properties such as the viscosity of the system used. The charge-transfer rate for most metal deposition reactions is sufficiently high of established nuclei to be mass transport controlled, so that the less viscous system should have the highest nuclear number density. The nucleation overpotential can be further evaluated using Zn|Zn coin cells to highlight this difference. In Aqueous electrolyte, the nucleation overpotential decreases from 190 mV in DESU0.3 and 180 mV in EG-based electrolytes to 70 mV. Although, dissolution of metal oxide in DES seems to be a common practice in metal electroplating few studies concerning the dissolution mechanisms and dissolved species are present. [78] Solubility of ZnO increases in the order $U > EG$ and this can be clearly seen in Fig. 21. This result fits well with the data reported in literature [79] even if a clear explanation of the influence of the HBD in the solvation mechanism was not reported. Similar to ILs, the availability of coordinating ligands appears to be important for the dissolution of metal oxides. The high solubility of transition-metal oxides is in some cases due to their ability to complex with urea, thus increasing their size and interaction with the solvent. When the ZnO dissolves in the deep eutectic solvent, the oxygen remains attached to the metal center and urea acts as a ligand forming $[ZnClO(urea)]^-$ [80]. Urea is a stronger HBD in comparison to ethylene glycol and its higher electronegativity can be used to explain the dissolution mechanism. Indeed, Zn is a late and hard metal that tends to form more stable complexes with hard ligand. We can then suppose that the coordination with a stronger ligand such as urea is more favorable. The milky white appearance of the ChEG with ZnO can be attributed to the formation of a stable colloidal suspension rather than a complete dissolution process. Ethylene glycol can act more like a suspending agent rather than forming a Zn complex. Indeed, some literature studies report the use of polyol for the preparation of metal-oxides nanoparticles yielding to colloidal stable suspension [81].

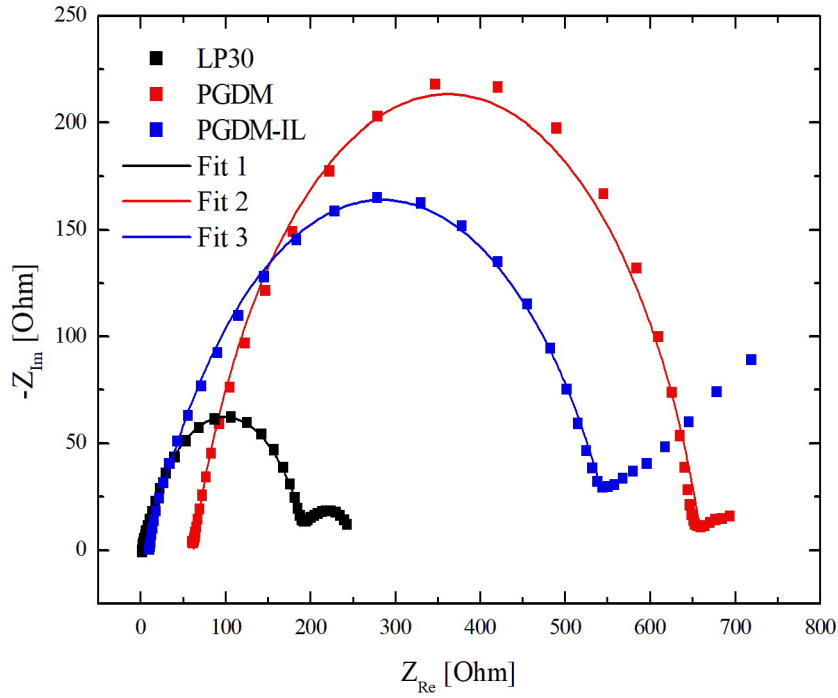
Given the above, the cell cycling behaviour can be explained. The higher solubility of ZnO in ChU leads U-series to have more regular transients and fail due to short circuit, while EG-series transients remain more irregular especially at high CDs, then failing due to passivation. This can be linked to the summary Tab. 3.

3.2. Lithium symmetrical cells

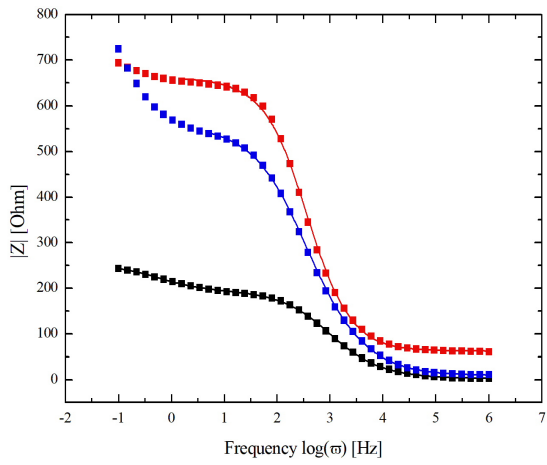
As seen in Section 1, the choice of the electrolyte can play a crucial role, developing suitable smart interfaces that extend the specific capacity of LIBs. Commercial LIBs are comprised of LiPF_6 in a mixture of carbonate solvents as the electrolyte [52]. When the cell operates, the anion present in lithium salt undergoes an equilibrium reaction and forms a Lewis acid PF_5 . This Lewis acid, in turn, reacts with the organic solvents EC/PC. The P–F bonds thus formed easily undergo hydrolysis, even if trace quantity of moisture is in the electrolyte medium, which, in turn, affects the performance of LIBs, hence making these solvents highly unsuitable [82]. Hence, in order to overcome the abovementioned issues, better alternatives of hydrophobic IL electrolytes are found to be one of the most promising electrolytes for LIBs, providing the stability for lithium electrode from air or moisture due to its hydrophobic-nature. ILs, with their high ionic conductivity, can act both as solvent and electrolyte: the incorporation of ILs into the electrolyte gives an efficient transport of Li^+ cations, favouring to simultaneously progress in safety, along with energy and power densities [83]. They consist of organic cations derivatives joined inorganic anions, respectively pyrrolidinium (Pyr) and bis(trifluoromethanesulfonyl imide) (TFSI) in our case. Polymer electrolytes satisfy numerous requirements, such as compatibility with the electrodes, no leakage, better thermal and appropriate mechanical stabilities. For this thesis, PEGDME was chosen and, to understand the behaviour of IL, we have proceeded with two different series, with and without IL. Finally, it is known that high temperature has a good impact on IL conductivity [84, 85], thus it was decided to cycle at 60 °C, both polymer-based series, in which LiTFSI was dissolved. The major challenge for IL-salt systems is the formation of crystalline phases, which limits further increase in the Li salt concentration. Using asymmetric anions – as TFSI – instead of the common symmetric ones can prevent crystallization and push the limiting Li salt concentration to higher values [86, 87]. However, Devaux et. al. [88] have shown a different way to weight Li salt, based on ethylene oxide group (EO) present in polymer electrolytes. The reason for this choice is related to the fact that the transport of Li is supported only by the chain of the EO ($-\text{OCH}_2\text{CH}_2-$)_n group.

3.2.1 EIS of pristine cells

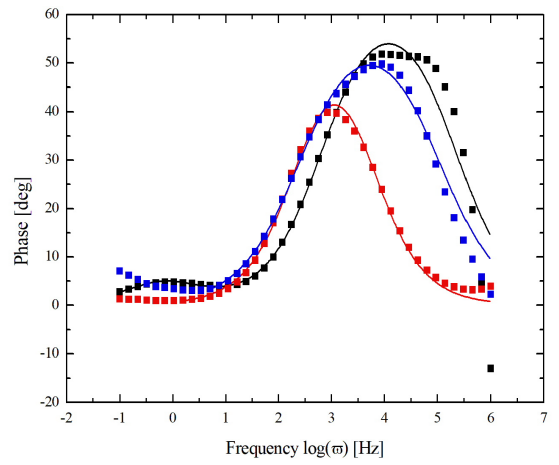
Six identical cells for each electrolyte type (LP30, PEGDME and PEGDME:Pyr14TFSI) were assembled to have three replicates for each current density (CD) condition: 0.1 and 10 mA cm^{-2} for EC/DMC, 0.05 and 1 mA cm^{-2} for PEGDME and PEGDME:Pyr14TFSI. As for Zn cells, EIS measurements were carried out in order to verify the correct assembly and test the electrochemical behaviour of the pristine cells. The EISs obtained are similar in shape and size: due to the high statistical quality of the data obtained, it is appropriate to represent the three cases with a single characteristic curve (Fig. 22). For simplicity, electrolytes are renamed as LP30, PGDM and PGDM-IL, respectively.



(a) Nyquist plot of Li electrolytes.



(b) Bode magnitude plot of Li electrolytes.



(c) Bode phase plot of Li electrolytes.

Figure 22: Pristine EISs of Li electrolytes.

Two different EECs models were used to characterize these behaviours (Fig. 23). As can be seen in both Fig. 22 and Fig. 23, not all series are characterized by a double capacitive-semicircle, which in the literature [89, 90] is considered as the series between the charge transfer effect and the formation of SEI. Where there is no real semicircle, the passive layer is formed by electrolyte decomposition, and passivation effect prevails: it has not been possible to follow the experimental data, since for those points at low frequencies the steady-state hypothesis, necessary to be able to apply the electrical similarity, fails.

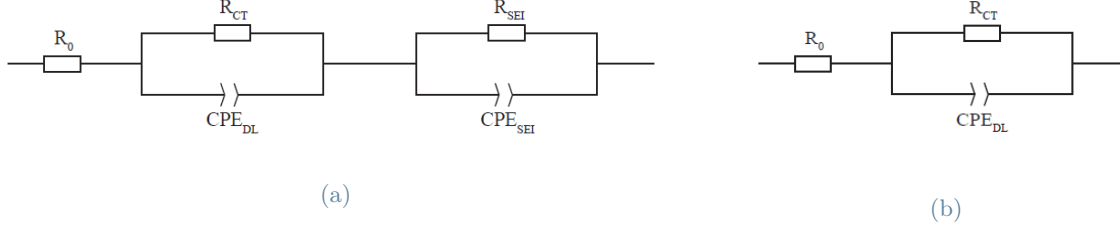


Figure 23: EECs for pristine Li EISs.

Tab. 5 shows the fitting results, while in Fig. 24 a representation of the passivation tails for the PGDM and PGDM-IL cases is shown, in order to compare the trend of the passivating effect over time.

	LP30	PGDM	PGDM-IL
R_o [Ω]	2.23 ± 0.65	60.56 ± 5.34	9.74 ± 0.90
R_{CT} [Ω]	187.38 ± 37.31	759.43 ± 238.07	676.34 ± 209.51
τ_{DL} [s]	$(1.68 \pm 0.47)e^{-3}$	$(3.57 \pm 0.86)e^{-3}$	$(5.19 \pm 1.13)e^{-3}$
α_{DL} [-]	0.762 ± 0.021	0.769 ± 0.026	0.729 ± 0.026
R_{SEI} [Ω]	39.66 ± 11.20	-	-
τ_{SEI} [s]	0.307 ± 0.095	-	-
α_{SEI} [-]	0.688 ± 0.059	-	-

Table 5: Fitting parameters of pristine Li EISs in terms of $\mu \pm \sigma$.

LP30 can be considered as the standard electrolyte in Li-ion battery research, exhibiting excellent cycling behaviour with low polarization and little propensity for dendritic growth [89], so it is not surprising to see that, compared to the other two series, it turns out to be the best electrolyte. It is therefore characterized by the lowest R_o and R_{CT} . Furthermore, the ability to form an efficient SEI is described by the presence of the second semicircle [89], which is missing in the other two cases. The two polymer-based electrolytes are characterized by a single capacitive-semicircle and the passivation tail, but they present some differences. First of all, R_o is completely different: polymer without IL has R_o larger than an order of magnitude respect to PGDM-IL. However, this is justified by the literature on ILs [54], which are used to increase the conductivity of the electrolyte. In our particular case, the polymeric electrolyte, PEGDME, is represented by highly viscose ethers, based on $(-OCH_2CH_2-)_n$ groups of short chain configuration [91]. Despite their promise in terms of suitable characteristics, previously listed, for application in lithium ion battery [92], these EO-based polymer still suffer from issues related to the stability of lithium metal-electrolyte interphase, leading to resistance increase and cell polarization [93]. This is the reason why PGDM experience the highest R_o and R_{CT} .

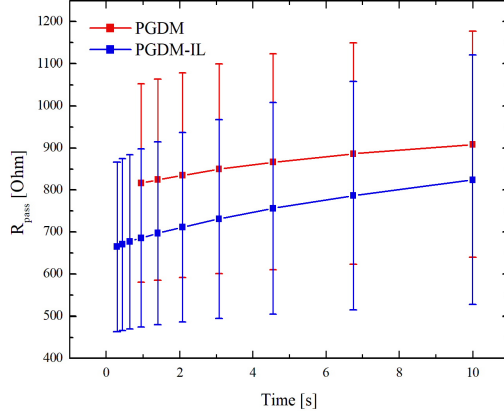


Figure 24: Passivation resistance over time.

As said previously, for polymer-based electrolytes it is not possible to fit the part at low frequency due to the formation of SEI. To avoid making a fitting, as in [89], where the fitting curves are reported but not the resulting parameters, it was preferred to proceed with a different analysis: the fitting was used for the points that allowed the analogy with EEC, while the passivation tail points were represented on R_{pass} -time graph [9] for the comparison of the two cases. As can be seen from Fig. 24, the formation of SEI is favored in the presence of Pyr14TFSI, since the effect begins to occur at lower times (higher frequencies). Also for the R_{pass} values, PGDM-IL seems favored, since the internal resistance of the cell is reduced.

3.2.2 GCD cycles

The CDs to which the three series have been cycled are different from each other: they do not correspond as in the case of the Zn cells. The choice was more or less forced by the fact that for the polymer-based electrolyte with IL there is still no sensitivity on their electrochemical window. Therefore it was decided to cycle the LP30 in its range [94]: 0.1 mA cm^{-2} and 10 mA cm^{-2} at 1 mAh cm^{-2} . For PGDM and PGDM-IL series the currents are much lower: 0.05 mA cm^{-2} and 1 mA cm^{-2} at 0.1 mAh cm^{-2} .

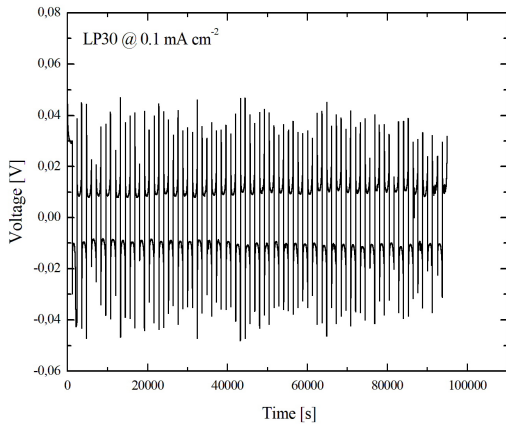


Figure 25: LP30 GCD at 0.1 mA cm^{-2}

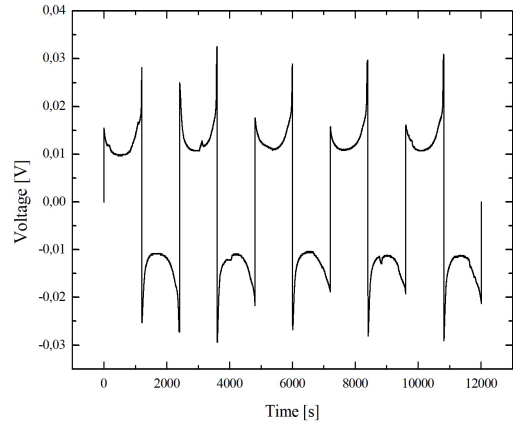


Figure 26: Chronopotentiometric transient of LP30 at 0.1 mA cm^{-2}

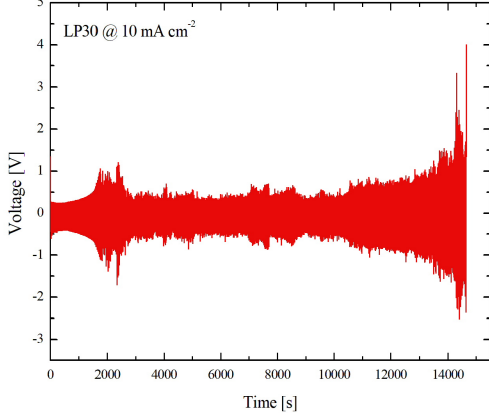


Figure 27: LP30 GCDC at 10 mA cm^{-2}

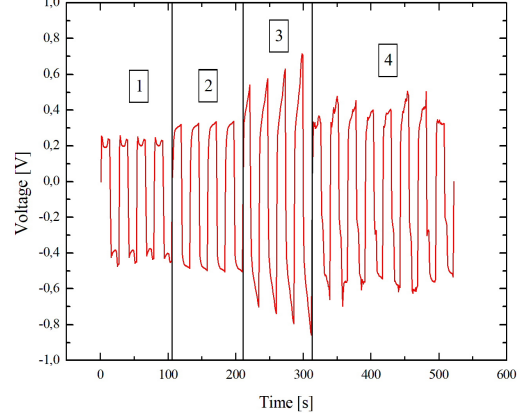


Figure 28: Chronopotentiometric transient of LP30 at 10 mA cm^{-2}

At 0.1 mA cm^{-2} , it was decided to run LP30 cells till 40 cycles (Fig. 25), in order to apply model reported in [3] and verify its validity. The global profile of this measurement remains confined between $\pm 45 \text{ mV}$ and has a flat shape without phenomena of surface outgrowth and passivation that modify the profile of the chronopotentiometric cycles, both for cathodic polarization (deposition) response and anodic polarization (dissolution) response. This behaviour implies a globally stable Li stripping/plating: phenomena as outgrowth and passivation are not present, thus $F_C = 0$ and $k_{\text{pass}} = 0$. The cycling stability of the Li metal electrode was determined using the interfacial stability between the Li surface and electrolyte. By looking the fast regime, after the first 2 ± 1 irregularly shaped charge-discharge cycles, the remaining transients have constant shape as shown in Fig. 26 with a parabolic-shape that suggests an outgrowth/stripping/outgrowth process during the single transient. According to [3], this parabolic form can be derived with values of: $D = 3e^{-5}$, $r_{\text{max}} = 0.1$ and $k_{\text{pass}} = 3.5e^{-6}$. At high CD, instead (Fig. 27), a complex scenario can be observed. The measurements start with a fairly regular and constant period of ca. 20 cycles, from which a growing profile begins to develop. After reaching a peak of $\pm 1 \text{ V}$, the amplitude of the transients begins to decrease until it reaches ca. $\pm 0.75 \text{ V}$. Eventually, all cells undergo a gradual increase until the cut-off voltage. If the fast regime is taken into account, it is observed that, for each period mentioned above, there is a specific form of the transients which describes the phenomena that occur. In Fig. 28 these shapes are shown. The starting period is characterized by a shape with a double peaks, similar to what happens at 0.1 mA cm^{-2} ; this trend last 17 ± 1 cycles. The period with the second shape lasts for 41 ± 8 cycles and it is characterized by a arc-shape and represents the moment when the potential profile begins to grow. The third one (12 ± 3 cycles) represents the last part of the growing period, before the descaling: the characterizing form is an elongated arc. The last period, on the other hand, is not characterized by any specific form; instead, it exhibits an irregular voltage variation with spikes, which is typical of non-uniform Li stripping/plating and dendrite formation [95]. The difference with low CD measurement can be attributed to the formation of lithium dendrites. This lithium dendrite formation is related to the interface state and reactivity between lithium and the electrolyte related to the current distribution during electrodeposition: higher CD, faster the dendrites formation [96, 97]. Aniruddha *et al.* [96] have shown that for very low current densities, stresses relax faster than the rate of electrodeposition and thus a planar electrodeposit is favoured; increasing CD, dendrite branches are promoted till the system becomes diffusion limited, inducing large concentration depletion gradients in front of the dendrite tip that result in tip-controlled growth.

Turning to the polymer-based series (Fig. 29, 30, 31, 32), the cycles at $C = 0.1 \text{ mAh cm}^{-2}$ are observed: cut-off voltage was set at $\pm 4 \text{ V}$, taking into account that the terminal $-\text{OH}$ group in PEG will be first oxidized when the voltage is higher than 4.05 V [98]. This is the main factor that limits the improvement of the electrochemical stability window. Moreover, the reactive $-\text{OH}$ group can react with the Li anode, which leads to poor Li stability. For PGDM, at low CD (Fig. 29) the voltage of the symmetric cells decreased from 60 mV to 10 mV in the first 80 h (20 cycles) and keeps stable at 10 mV after that, which implies the good electrochemical stability between the PEGDME and the Li metal anode. These results also indicate a great electrolyte|electrode interface contact. However, this occurs after progressive growth due to the passivated electrode in the first 7 cycles. For the measurement at high CD (Fig. 32), it is visible a symmetric behaviour, as for the previous case; however, the whole profile is not regular but it manifests decrease and increase sections. The behaviour at the transient level is very irregular throughout the whole period: a remarkable unstable, noisy and erratic profile is evidenced. This issue may be attributed to the formation of an unstable SEI over the lithium surface, which causes continuous electrolyte consumption and, therefore, very poor stability performance.

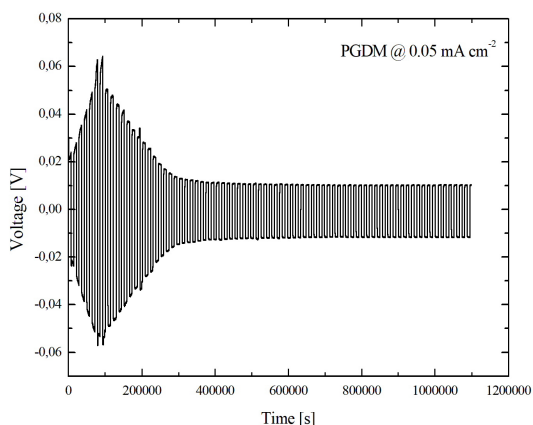


Figure 29: LP30 cycle at 0.1 mA cm^{-2}

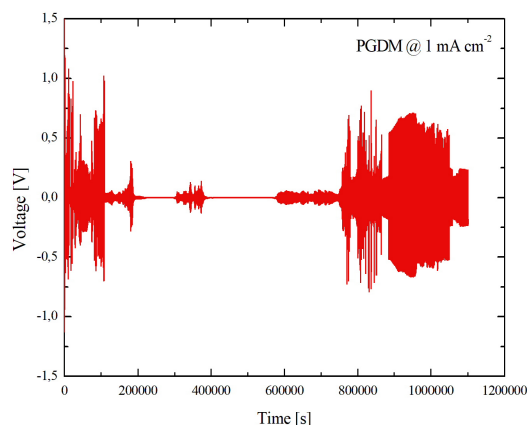


Figure 30: LP30 transient at 0.1 mA cm^{-2}

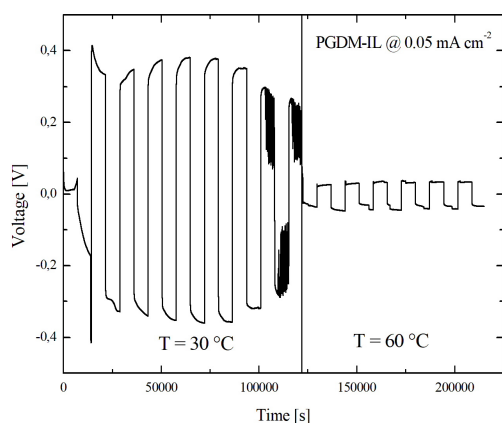


Figure 31: LP30 cycle at 10 mA cm^{-2}

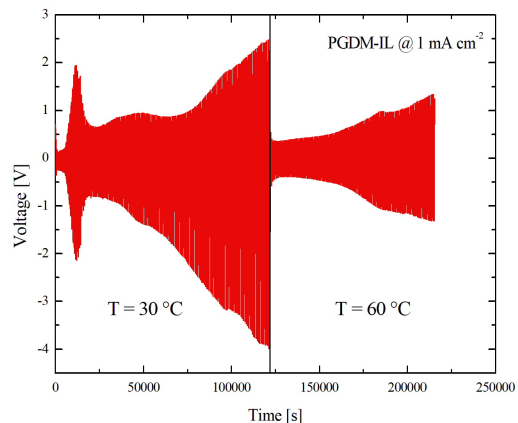


Figure 32: LP30 transient at 10 mA cm^{-2}

On the other hand, Fig. 31 and 32 show the two cycles of PGDM-IL. As it can be seen, due to technical problems, the first two days ca. measurements were recorded at $30 \text{ }^\circ\text{C}$ instead of $60 \text{ }^\circ\text{C}$. However, this displays the expected effect of temperature on IL. It is known that by increasing the temperature, the conductivity of the IL increases, at the same time decreasing the viscosity of the electrolyte. This is also demonstrated applying [3], because the period characterized by temperature of $30 \text{ }^\circ\text{C}$ is represented by chronopotentiometric transients that suggest low diffusivity, respect to the second part, characterized by higher temperature.

Even if the measurements between PGDM and PGDM-IL are reported with a different cycle time – PGDM-IL has been cycled successively – it is observed that, comparing Fig. 30 and 32 at the same cycle time, it is found that the mixture with IL has good compatibility with Li metal electrodes as demonstrated by impedance and galvanostatic Li stripping/deposition measurements.

3.2.3 EIS of aged cells

Since the polymer-based cells are still cycling, the only aged EIS reported is that for LP30. In Fig. 33, it can be seen that the effect of passivation is also observed for Li, even if, for LP30 case, dispersion is limited compared with Zn results. However, this is confirmed by the fact that many Li cells were terminated before death - those at 0.1 mA cm^{-2} - and the EIS measurement was performed immediately, reducing possible passivation effects. Nonetheless, the conjecture of passivation as a dominant effect for terminated cells has been made more solid, and this will be verify with a dedicated experiment following a calendar-ageing.

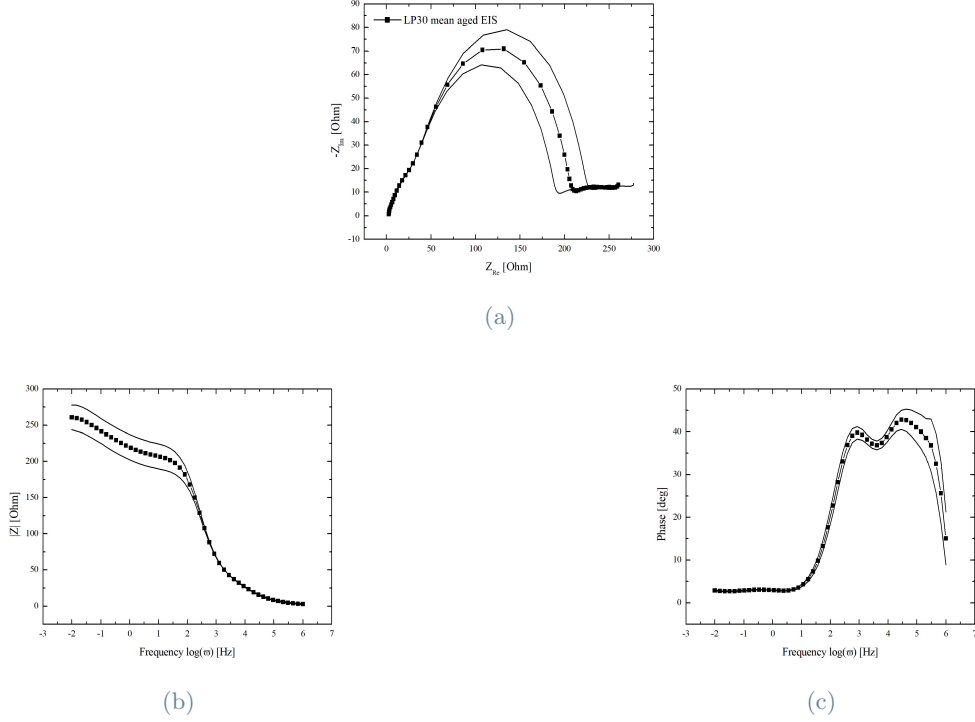


Figure 33: Dispersion of LP30 aged EISs.

For fitting process, the same model presented for pristine EISs (Fig. 23), was used. Results are shown in Tab. 6.

LP30	
R_o [Ω]	3.56 ± 0.61
R_{CT} [Ω]	37.23 ± 0.84
τ_{DL} [s]	$(6.78 \pm 0.14)e^{-4}$
α_{DL} [-]	0.675 ± 0.001
R_{SEI} [Ω]	170.61 ± 25.54
τ_{SEI} [s]	$(1.98 \pm 0.23)e^{-3}$
α_{SEI} [-]	0.867 ± 0.001

Table 6: Fitting parameters of pristine Li EISs in terms of $\mu \pm \sigma$.

4. Conclusion

A systematic characterization of the pristine EIS was made, coupling chemical-physical information of the new materials, the shape of the curve and the results of the fitting process. The graduation of the electrolytes was successful, concluding that from the point of view of the EIS, the AQ series for Zn and LP30 for Li are the most promising. However, as shown by EIS analyses of cells that have reached the end of life, regardless of the failure mode or the specific chemistry, all aged cells show passivation as the final outcome of calendar-aging - not shown in this thesis due to the unavailability of data due to technical problems, but which will be reported in a later version -, the quantitative aspects of which depend on the type of electrode and electrolyte.

Zn GCDC shows that ChU0.3 allows the best stability in terms of durability and repeatability of the chronopotentiometric transient, while ChEG gives rise to passivation and shows instability inside the transient at high CDs. For Li, relatively good behaviour of LP30 was found, in comparison with polymer- and IL-based systems. However, data of polymer-based electrolytes are uncompleted, but it is possible to conclude that polymer-based

solution without IL has not good physic-chemical properties to create a performing electrolyte. Furthermore, thanks to the technical problem, we have also seen the effect that temperature has on IL, showing a incredible resistance reduction due to the increase of conductivity. However, the behavior during reduction and oxidation of Li in PEGDME:LiTFSI:Pyr14TFSI is poorly reported in the literature, which makes further investigation on the mechanisms of the system difficult.

In conclusion, morphochemical modelling of GCDC time-series allowed a transparent rationalization of the observed electrochemical performance and SEM microscopy in terms of simple, but highly diagnostic physico-chemical parameters, as exemplified in Tab. 7 for a prototypical case, or GCDCs dominated by diffusive effects (parameter D) and micromorphology controlled by the number density of nuclei (parameter r_{\max}).

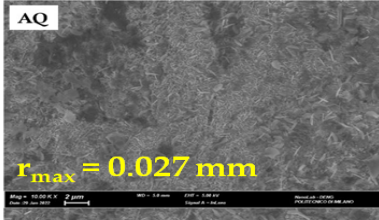
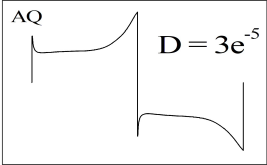
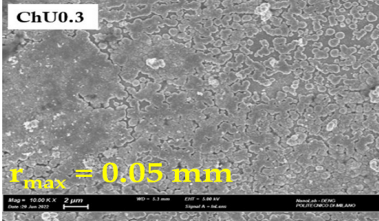
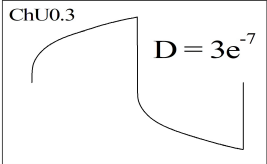
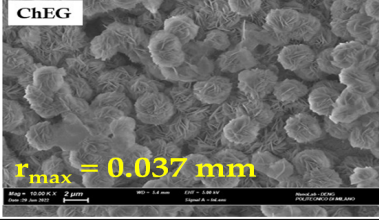
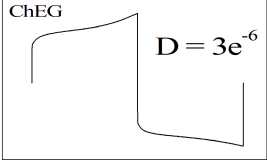
	SEM/ r_{\max}	transient/ D
AQ		
ChU0.3		
ChEG		

Table 7: Comparison between experimental data (SEM scans and transients) and obtained results (D and r_{\max}).

References

- [1] D. Applestone and A. Manthiram, "Symmetric cell evaluation of the effects of electrolyte additives on $\text{Cu}_2\text{Sb}-\text{Al}_2\text{O}_3-\text{C}$ nanocomposite anodes," *Journal of Power Sources*, 2012, 217, 1-5.
- [2] J. C. Burns, L. J. Krause, D.-B. Le, L. D. Jensen, D. X. A. J. Smith, and J. R. Dahna, "Introducing symmetric li-ion cells as a tool to study cell degradation mechanisms," *Journal of The Electrochemical Society*, 2011, 158 (12) A1417-A1422.
- [3] F. Rossi, L. Mancini, I. Sgura, M. Boniardi, A. Casaroli, A. P. Kao, and B. Bozzini, "Insight into the cycling behaviour of metal anodes, enabled by x-ray tomography and mathematical modelling," *ChemElectroChem*, 2022, 9, e202101537 (1 of 8).
- [4] R. Petibon, C. P. Aiken, N. N. Sinha, J. C. Burns, H. Ye, C. M. VanElzen, G. Jain, S. Trussler, and J. R. Dahna, "Study of electrolyte additives using electrochemical impedance spectroscopy on symmetric cells," *Journal of The Electrochemical Society*, 2013, 160 (1) A117-A124.
- [5] K. Wang, X. Zhang, J. Han, X. Zhang, X. Sun, a. L. C. Li, Q. Li, and Y. Ma, "High-performance cable-type

- flexible rechargeable zn battery based on $\text{mno}_2@\text{cnt}$ fiber microelectrode,” *ACS Appl. Mater. Interfaces*, 2018, 10, 29, 24573-24582.
- [6] W. Kao-ian, R. Pornprasertsuk, P. Thamyongkit, T. Maiyalagan, and S. Kheawhom, “Rechargeable zinc-ion battery based on choline chloride-urea deep eutectic solvent,” *Journal of The Electrochemical Society*, 2019, 166 (6) A1063-A1069.
- [7] C. R. R. Kumara, P. Kotteeswaranb, V. B. Rajud, A. Muruganb, M. S. Santoshf, H. P. Nagaswarupaa, S. C. Prashantha, M. R. A. Kumara, and M. S. Shivakumarg, “Influence of zinc additive and ph on the electrochemical activities of β -nickel hydroxide materials and its applications in secondary batteries,” *Journal of Energy Storage*, 2017, 9 12–24.
- [8] R. I. Revilla, B. Wouters, F. Andreatta, A. Lanzutti, L. Fedrizzi, and I. D. Graevea, “Eis comparative study and critical equivalent electrical circuit (eec) analysis of the native oxide layer of additive manufactured and wrought 316l stainless steel,” *Corrosion Science*, 2020, 167 108480.
- [9] S. S. Zhang and D. T. Tran, “A simple approach for superior performance of lithium/sulphur batteries modified with a gel polymer electrolyte,” *J. Mater. Chem. A*, 2014, 2, 7383.
- [10] D. D. Lecce, V. Marangon, H.-G. Jung, Y. Tominaga, S. Greenbaum, and J. Hassoun, “Glyme-based electrolytes: suitable solutions for next-generation lithium batteries,” *Green Chem.*, 2022, 24, 1021.
- [11] K. il Chung, W.-S. Kim, and Y.-K. Choi, “Lithium phosphorous oxynitride as a passive layer for anodes in lithium secondary batteries,” *Journal of Electroanalytical Chemistry*, 2004, 566 263–267.
- [12] G. A. Elia, R. Bernhard, and J. Hassoun, “A lithium-ion oxygen battery using a polyethylene glyme electrolyte mixed with an ionic liquid,” *RSC Adv.*, 2015, 5, 21360.
- [13] S.-C. Wu, M.-C. Tsai, H.-J. Liao, T.-Y. Su, S.-Y. Tang, C.-W. Chen, H.-A. Lo, T.-Y. Yang, K. Wang, Y. Ai, Y.-Z. Chen, L. Lee, J.-F. Lee, C.-J. Lin, B. J. Hwang, and Y.-L. Chueh, “Intercalation of zinc monochloride cations by deep eutectic solvents for high-performance rechargeable non-aqueous zinc ion batteries,” *ACS Appl. Mater. Interfaces*, 2022, 14, 78147825.
- [14] A. G. Miranda and C. W. Hong, “Integrated modeling for the cyclic behavior of high power li-ion batteries under extended operating conditions,” *Applied Energy*, 2013, 111 681–689.
- [15] K.-H. Chen, K. N. Wood, E. Kazyak, W. S. L. Page, A. L. Davis, A. J. Sanchez, and N. P. Dasgupta, “Dead lithium: mass transport effects on voltage, capacity, and failure of lithium metal anodes,” *J. Mater. Chem. A*, 2017, 5, 11671.
- [16] Z. Yi, G. Chen, F. Hou, L. Wang, and J. Liang, “Strategies for the stabilization of zn metal anodes for zn-ion batteries,” *Adv. Energy Mater.*, 2021, 11 2003065.
- [17] P. Zou, Y. Sui, H. C. Zhan, C. Wang, H. L. Xin, H.-M. Cheng, F. Kang, and C. Yang, “Self-formed hybrid interphase layer on lithium metal for high-performance lithium–sulfur batteries,” *Chem. Rev.*, 2021, 121, 59866056.
- [18] X. G. Zhang, “Corrosion and electrochemistry of zinc,” 2013.
- [19] F. Wan and Z. Q. Niu, “Design strategies for vanadium-based aqueous zinc-ion batteries,” *Angew. Chem.*, 2019, 58, 16358.
- [20] H. B. Geng, M. Cheng, B. Wang, Y. Yang, Y. F. Zhang, and C. C. Li, “Strategies for the stabilization of zn metal anodes for zn-ion batteries,” *Adv. Funct. Mater.*, 2020, 30, 1907684.
- [21] F. Rossi, E. Marini, M. Boniardi, A. Casaroli, A. L. Bassi, A. Macrelli, C. Mele, and B. Bozzini, “What happens to mno_2 when it comes in contact with zn? an electrochemical study in aid of zn/ mno_2 -based rechargeable batteries,” *Energy Technology*, 2022, 10.1002/ente.202200084.
- [22] C. J. Xu, B. H. Li, H. D. Du, and F. Y. Kang, “Energetic zinc ion chemistry: The rechargeable zinc ion battery,” *Angew. Chem.*, 2012, 51 933.
- [23] F. Wan and Z. Q. Niu, “Design strategies for vanadium-based aqueous zinc-ion batteries,” *Angew. Chem.*, 2019, 58 16358.

- [24] R. Y. Wang, D. W. Kirk, and G. X. Zhang, "Effects of deposition conditions on the morphology of zinc deposits from alkaline zincate solutions," *Journal of The Electrochemical Society*, 2006, 153 5 C357-C364.
- [25] D. P. Trudgeon, X. L. K. Qiu, T. Mallick, O. O. Taiwo, B. Chakrabarti, V. Yufit, N. P. Brandon, D. Crevillen-Garcia, and A. Shah, "Redox flow batteries: Status and perspective towards sustainable stationary energy storage," *J. Power Sources*, 2019, 412, 44–54.
- [26] W. Lu, C. Xie, H. Zhang, and X. Li, "Inhibition of zinc dendrite growth in zinc-based batteries," *ChemSusChem*, 2018, 11, 3996–4006.
- [27] J. Liang, Z. H. Sun, F. Li, and H. M. Cheng *Energy Storage Mater.*, 2016, 2, 76-106.
- [28] L. Ma and C. Zhi, "Zn electrode/electrolyte interfaces of zn batteries: A mini review," *Electrochemistry Communications*, 2021, 122 106898.
- [29] L. Su, L. Liu, B. Liu, J. Meng, and X. Yan, "Revealing the impact of oxygen dissolved in electrolytes on aqueous zinc-ion batteries," *iScience*, 2020, 23, 100995.
- [30] E. Grignon, A. M. Battaglia, T. B. Schon, and D. S. Seferos, "Aqueous zinc batteries: Design principles toward organic cathodes for grid applications," *iScience*, 2022, 25, 104204.
- [31] F. Rossi, C. Mele, M. Boniardi, and B. Bozzini, "Electrodeposition of zinc from alkaline electrolytes containing quaternary ammonium salts and ionomers: Impact of cathodic-anodic cycling conditions," *ChemElectroChem*, 2020, 10.1002/celec.202000165.
- [32] G. D. Wilcox and P. J. Mitchell, "Electrolyte additives for zinc-anoded secondary cells ii. quaternary ammonium compounds," *Journal of Power Sources*, 1990, 32, 31-41.
- [33] C. Cachet, F. Ganne, G. Maurin, J. Petitjean, V. Vivier, and R. Wiart, "Eis investigation of zinc dissolution in aerated sulfate medium. part i: bulk zinc," *Electrochimica Acta*, 2001, 47, 3, 509-518.
- [34] W. Wang and D. B. Breisinger, "The acid-base behavior of zinc sulfate electrolytes: The temperature effect," *Metallurgical and Materials Transactions B*, 1998, 29, 1157–1166.
- [35] W. Wang, C. Yang, X. Chi, J. Liu, B. Wen, and Y. Liu, "Small-molecular crowding electrolyte enables high-voltage and high-rate supercapacitors," *Energy Technology*, 2021, 10.1002/ente.202100684.
- [36] E. L. Smith, A. P. Abbott, and K. S. Ryder, "Deep eutectic solvents (dess) and their applications," *Chemical Reviews*, 2014, 114, 11060-11082.
- [37] A. P. Abbott, G. Capper, D. L. Davies, H. L. Munro, R. K. Rasheed, and V. Tambyrajah, "Preparation of novel, moisture-stable, lewis-acidic ionic liquids containing quaternary ammonium salts with functional side chains," *Chem. Commun.*, 2001, 2010-2011.
- [38] A. P. Abbott, J. C. Barron, K. S. Ryder, and D. Wilson, "Eutectic-based ionic liquids with metal-containing anions and cations," *Chemistry.*, 2007, 13.
- [39] A. P. Abbott, A. A. Al-Barzinjy, P. D. Abbott, G. Frisch, R. C. Harris, J. Hartley, and K. S. Ryder, "Speciation, physical and electrolytic properties of eutectic mixtures based on $\text{CrCl}_3 \cdot 6\text{H}_2\text{O}$ and urea," *Phys. Chem. Chem. Phys.*, 2014, 16, 9047-9055.
- [40] K. Ghandi, "A review of ionic liquids, their limits and applications," *GreenSustain. Chem.*, 2014, 4 44–53.
- [41] T. P. T. Pham, C. W. Cho, and Y. S. Yun, "Environmental fate and toxicity of ionic liquids: A review," *Water Res.*, 2010, 44, 352–372.
- [42] L. I. N. Tomé, V. Baião, W. da Silva, and C. M. A. Brett, "Deep eutectic solvents for the production and application of new materials," *Applied Materials Today*, 2018, 10, 30–50.
- [43] C. Ma, A. Laaksonen, C. Liu, X. Lu, and X. Ji, "The peculiar effect of water on ionic liquids and deep eutectic solvents," *Chem. Soc. Rev.*, 2018, 47, 8685.
- [44] R. K. Ibrahim, M. Hayyan, M. A. AlSaadi, S. Ibrahima, A. Hayyan, and M. A. Hashim, "Removal of thiophene from mixtures with n-heptane by selective extraction using deep eutectic solvents," *Journal of Molecular Liquids*, 2019, 276 794–800.

- [45] M. Figueiredo, C. Gomes, R. Costa, A. Martins, C. M. Pereira, and F. Silva, "Differential capacity of a deep eutectic solvent based on choline chloride and glycerol on solid electrodes," *Electrochimica Acta*, 2009, 54 2630–2634.
- [46] R. Costa, M. Figueiredo, C. M. Pereira, and F. Silva, "Differential capacity of a deep eutectic solvent based on choline chloride and glycerol on solid electrodes," *Electrochimica Acta*, 2010, 55 8916–8920, 52.
- [47] "Eu battery demand and supply (2019-2030) in a global context," *Avicenne Energy*, 2021.
- [48] J. Lu, Z. Chen, F. Pan, Y. Cui, and K. Amine, "High-performance anode materials for rechargeable lithium-ion batteries," *Electrochem. Energy Rev.*, 2018, 1, 3553.
- [49] N. D. Trinh, D. Lepage, D. Ayme-Perrot, A. Badia, M. Dolle, and D. Rochefort, "An artificial lithium protective layer that enables the use of acetonitrile-based electrolytes in lithium metal batteries," *Angew. Chem.*, 2018, 57, 50725075.
- [50] Z. Wang, Z. Sun, J. Li, Y. Shi, C. Sun, B. An, H. M. Cheng, and F. Li, "Insights into the deposition chemistry of li ions in nonaqueous electrolyte for stable li anodes," *Chem. Soc. Rev.*, 2021, 50 3178–3210.
- [51] S. J. An, J. Li, D. M. Claus Daniel, S. Nagpure, and D. L. W. III, "Cheminform abstract: The state of understanding of the lithium-ion-battery graphite solid electrolyte interphase (sei) and its relationship to formation cycling," *Carbon*, 2016, 105 52e76.
- [52] L. Meyer, D. Curran, R. Brow, S. Santhanagopalan, and J. Porter, "Operando measurements of electrolyte li-ion concentration during fast charging with ftir/atr," *J. Electrochem. Soc.*, 2021, 168, 090502.
- [53] K. Karuppasamy, J. Theerthagiri, D. Vikraman, C. J. Yim, S. Hussain, R. Sharma, T. Maiyalagan, J. Qin, and H. S. Kim, "Ionic liquid-based electrolytes for energy storage devices: A brief review on their limits and applications," *Polymers*, 2020, 12 918.
- [54] E. Pargoletti, S. Arnaboldi, G. Cappelletti, M. Longhi, D. Meroni, A. Minguzzi, P. R. Mussini, S. Rondinini, and A. Vertova, "Smart interfaces in li-ion batteries: near-future key challenges," *Electrochimica Acta*, 2022, 415, 140258.
- [55] A. Balducci, "Ionic liquids in lithium-ion batteries," *Top Curr Chem*, 2017, (Z) 375:20.
- [56] A. Eftekhari, Y. Liu, and P. Chen, "Different roles of ionic liquids in lithium batteries," *Journal of Power Sources*, 2016, 334 221-239.
- [57] I. Osada, H. de Vries, B. Scrosati, and S. Passerini, "Ionic-liquid-based polymer electrolytes for battery applications," *Angew. Chem. Int. Ed.*, 2016, 55, 500–513.
- [58] K. M. Abraham, Z. Jiang, and B. Carroll, "Highly conductive peo-like polymer electrolytes," *Chem. Mater.*, 1997, 9, 1978-1988.
- [59] Y. Kanga, H. J. Kima, E. Kima, B. Ohb, and J. H. Choc, "Photocured peo-based solid polymer electrolyte and its application to lithium-polymer batteries," *Journal of Power Sources*, 2001, 92 255–259.
- [60] H. Wang, D. Im, D. J. Lee, M. Matsui, Y. Takeda, O. Yamamoto, and N. Imanishia, "A composite polymer electrolyte protect layer between lithium and water stable ceramics for aqueous lithium-air batteries," *Journal of The Electrochemical Society*, 2013, 160 (4) A728-A733.
- [61] M. Montanino, M. Moreno, F. Alessandrini, G. B. Appetecchi, S. Passerini, Q. Zhou, and W. A. Henderson, "Physical and electrochemical properties of binary ionic liquid mixtures: (1x) pyr14tfsi-(x) pyr14im14," *Electrochimica Acta*, 2012, 60 163–169.
- [62] M. Nádherná, J. Reiter, J. Moškon, and R. Dominko, "Lithium bis(fluorosulfonyl)imide-pyr14tfsi ionic liquid electrolyte compatible with graphite," *Journal of Power Sources*, 2011, 196, 7700-7706.
- [63] M. Montanino, M. Moreno, M. Carewska, G. Maresca, E. Simonetti, R. L. Presti, F. Alessandrini, and G. B. Appetecchi, "Mixed organic compound-ionic liquid electrolytes for lithium battery electrolyte systems," *Journal of Power Sources*, 2014, 269 608-615.
- [64] T. Zhekenov, N. Toksanbayev, Z. Kazakbayeva, D. Shah, and F. S. Mjalli, "Formation of type iii deep eutectic solvents and effect of water on their intermolecular interactions," *Fluid Phase Equilibria*, 2017, 441 43e48.

- [65] T. Caielli, "Zn anode shape-change suppression in mildly acidic aqueous zinc-ion battery electrolytes containing quaternary ammonium salts," *Politecnico di Milano*, 2021.
- [66] M. de Pauli, A. M. Gomes, R. L. Cavalcante, R. B. Serpa, C. P. Reis, F. T. Reis, and M. L. Sartorelli, "Capacitance spectra extracted from eis by a model-free generalized phase element analysis," *Electrochimica Acta*, 2019, 320 134366.
- [67] J. R. Macdonald, "Frequency response of unified dielectric and conductive systems involving an exponential distribution of activation energies," *Journal of Applied Physics*, 1985, 58 (5).
- [68] D. P. Almond and A. R. West, "Complex impedance plane plots and the determination of conductivities of "real" dispersive conductors," *J Electroanal Chem*, 1985, 186 17-25.
- [69] A. K. Jonscher, "The universal dielectric response," *IEEE Electrical Insulation Magazine*, 1990, 6, 2.
- [70] B. Hirschorn, M. E. Orazem, B. Tribollet, V. Vivierb, I. Frateurc, and M. Musianid, "Determination of effective capacitance and film thickness from constant-phase-element parameters," *Electrochimica Acta*, 2010, 55 6218–6227.
- [71] Z. Chen, B. McLean, M. Ludwig, R. Stefanovic, G. G. Warr, G. B. Webber, A. J. Page, and R. Atki, "Nanostructure of deep eutectic solvents at graphite electrode interfaces as a function of potential," *J. Phys. Chem.*, 2016, 120, 22252233.
- [72] L. Vieira, R. Schennach, and B. Gollas, "The effect of the electrode material on the electrodeposition of zinc from deep eutectic solvents," *Electrochimica Acta*, 2016 197 344–352.
- [73] C. M. A. Laaksonen, C. Liu, X. Lu, and X. Ji, "The peculiar effect of water on ionic liquids and deep eutectic solvents," *Chem. Soc. Rev.*, 2018,47, 8685.
- [74] A. P. Abbott, J. C. Barron, G. Frisch, S. Gurman, K. S. Ryder, and A. F. Silva, "Double layer effects on metal nucleation in deep eutectic solvents," *Phys. Chem. Chem. Phys.*, 2011, 13, 10224-10231.
- [75] J. Shi, T. Sun, J. Bao, S. Zheng, H. Du, L. Li, X. Yuan, T. Ma, and Z. Tao, "Water-in-deep eutectic solvent electrolytes for high-performance aqueous zn-ion batteries," *Funct. Mater.*, 2021, 31, 2102035.
- [76] J. Y. Kim, G. Liu, H. K. Ga Young Shim, and J. K. Lee, "Functionalized zn@zno hexagonal pyramid array for dendrite-free and ultrastable zinc metal anodes," *Adv. Funct. Mater.*, 2020, 2004210.
- [77] Q. Zhang, Z. Yang, H. Ji, X. Zeng, Y. Tang, D. Sun, and H. Wang, "Issues and rational design of aqueous electrolyte for zn-ion batteries," *SusMat.*, 2021, 1:432–447.
- [78] J. Richter and M. Ruck, "Synthesis and dissolution of metal oxides in ionic liquids and deep eutectic solvents," *Molecules*, 2020, 25, 78.
- [79] A. P. Abbott, G. Capper, D. L. Davies, K. J. McKenzie, and S. U. Obi, "Solubility of metal oxides in deep eutectic solvents based on choline chloride," *J. Chem. Eng. Data*, 2006, 51, 1280-1282.
- [80] A. P. Abbott, G. Capper, D. L. Davies, R. K. Rasheed, and P. Shikotra, "Selective extraction of metals from mixed oxide matrixes using choline-based ionic liquids," *Inorganic Chemistry*, 2005, 44, 19.
- [81] C. Feldmann, "Polyol-mediated synthesis of nanoscale functional materials," *Adv. Funct. Mater.*, 2003, 13, 2, 101-107.
- [82] K. Karupphasamy, J. Theerthagiri, D. Vikraman, C.-J. Yim, S. Hussain, R. Sharma, T. Maiyalagan, J. Qin, and H.-S. Kim, "Ionic liquid-based electrolytes for energy storage devices: A brief review on their limits and applications," *Polymers*, 2020, 12, 918.
- [83] I. Osada, H. de Vries, B. Scrosati, and S. Passerini, "Ionic-liquid-based polymer electrolytes for battery applications," *Angew. Chem.*, 2016, 55, 500–513.
- [84] J. Vila, P. Ginés, J. M. Pico, C. Franjo, E. Jiménez, L. M. Varela, and O. Cabeza, "Temperature dependence of the electrical conductivity in emim-based ionic liquids evidence of vogel tamman fulcher behavior," *Fluid Phase Equilibria*, 2006, 242 141–146.
- [85] M. Nadherna, J. Reitera, J. Moskon, and R. Dominko, "A bilayer polymer electrolyte encompassing pyrrolidinium-based rtil for binder-free silicon few-layer graphene nanocomposite anodes for li-ion battery," *Journal of Power Sources*, 2011, 196 7700– 7706.

- [86] W. A. Henderson and S. Passerini, "Phase behavior of ionic liquid mixtures: pyrrolidinium cations and tfsi- anions," *Chem. Mater.*, 2004, 16, 2881.
- [87] J. Tong, S. Wu, N. von Solms, X. Liang, F. Huo, Q. Zhou, H. He, and S. Zhang, "The effect of concentration of lithium salt on the structural and transport properties of ionic liquid-based electrolytes," *Front. Chem.*, 2020, 7:945.
- [88] D. Devaux, R. Bouchet, D. Glé, and R. Denoyel, "Mechanism of ion transport in peo/litfsi complexes: Effect of temperature, molecular weight and end groups," *Solid State Ionics*, 2012, 227, 119–127.
- [89] D. I. Iermakova, R. Dugas, M. R. Palacín, and A. Ponrouch, "On the comparative stability of li and na metal anode interfaces in conventional alkyl carbonate electrolytes," *Journal of The Electrochemical Society*, 2015, 162 (13) A7060-A7066.
- [90] S. Zhang, K. Xu, and T. Jow, "Eis study on the formation of solid electrolyte interface in li-ion battery," *Electrochimica Acta*, 2006, 51 1636–1640.
- [91] G. A. Elia, R. Bernhard, and J. Hassoun, "A lithium-ion oxygen battery using a polyethylene glyme electrolyte mixed with an ionic liquid," *RSC Advances*, 2015, 5, 21360-21365.
- [92] R. Bernhard, A. Latini, S. Panero, B. Scrosati, and J. Hassoun, "Poly(ethylenglycol)dimethylether–lithium bis(trifluoromethanesulfonyl)imide, peg500dme–litfsi, as high viscosity electrolyte for lithium ion batteries," *J. Power Sources*, 2013, 226, 329-333.
- [93] S. S. Zhang, "Liquid electrolyte lithium/sulfur battery: Fundamental chemistry, problems, and solutions," *J. Power Sources*, 2013, 231, 153-162.
- [94] H. Kühnle, E. Knobbe, and E. Figgemeier, "In situ optical and electrochemical investigations of lithium depositions as a function of current densities," *Journal of The Electrochemical Society*, 2022, 169 040528.
- [95] K.-I. Chung, W.-S. Kim, and Y.-K. Choi, "Recent advances in the development of li-air batteries," *J. Electroanal. Chem.*, 2004, 566 263e267.
- [96] A. Jana, S. I. Woo, K. S. N. Vikrant, and R. E. García, "Electrochemomechanics of lithium dendrite growth," *Energy Environ. Sci.*, 2019, 12, 3595.
- [97] I. W. Seong, C. H. Hong, B. K. Kim, and W. Y. Yoon, "The effects of current density and amount of discharge on dendrite formation in the lithium powder anode electrode," *Journal of Power Sources*, 2008, 178 769–773.
- [98] X. Yang, M. Jiang, X. Gao, D. Bao, Q. Sun, N. Holmes, H. Duan, S. Mukherjee, K. Adair, C. Zhao, J. Liang, W. Li, J. Li, Y. Liu, H. Huang, L. Zhang, S. Lu, Q. Lu, R. Li, C. V. Singh, and X. Sun, "Determining the limiting factor of the electrochemical stability window for peo-based solid polymer electrolytes: main chain or terminal -oh group?," *Energy Environ. Sci.*, 2020, 13, 1318.

Abstract in lingua italiana

Le celle simmetriche sono uno strumento molto importante per l'analisi dei materiali delle batterie, permettendo lo studio di sistemi elettrodi/elettroliti in condizioni operative realistiche. Studi rigorosi sui cambiamenti di forma dell'anodo metallico della batteria durante il ciclo sono rari ma particolarmente importanti per sviluppare un'implementazione affidabile e duratura dei materiali. Tuttavia, manca ancora una "cassetta degli attrezzi" – sia concettuale che sperimentale – per lo studio rigoroso di questi sistemi. Pertanto, l'obiettivo di questa tesi è lo studio dei problemi di cambiamento di forma e passivazione di anodi metallici in condizioni operative reali. Questo studio si basa sulla combinazione sistematica di dati sperimentali di elevata qualità statistica con nuovi studi, che si sono posti l'obiettivo di descrivere i profili dei transitori cronopotenziometrici attraverso modelli che descrivono la risposta elettrochimica tramite parametri elettrocinetici, di trasporto di massa e di evoluzione dei materiali. Questo approccio non è comune in letteratura: le risposte anodiche e catodiche sono generalmente studiate isolatamente e, d'altra parte, quando si considerano i dati del ciclo, l'uso quantitativo di serie temporali elettrochimiche è molto raro e viene preso in considerazione solo il tempo di fallimento. Inoltre, questa tesi studia il comportamento di nuovi materiali elettrolitici per batterie Zn e Li. Per quanto riguarda Zn, la prospettiva chiave è quella di passare da ambienti alcalini a elettroliti acquosi a bassa acidità. Nello specifico, abbiamo affrontato l'argomento scarsamente studiato degli additivi organici per la soppressione della crescita dei dendriti, in particolare il sale di ammonio quaternario (QAS). Inoltre, abbiamo studiato i Deep Eutectic Solvents (DESs), come possibile sostituzione di soluzioni acquose, formati da un QAS e da un donatore di legame idrogeno. Per quanto riguarda Li, abbiamo considerato il tradizionale elettrolita LP30 come punto di riferimento, rispetto al quale abbiamo testato un elettrolita a base polimerico e una miscela polimero/IL.

Parole chiave: celle simmetriche, ciclo, cambiamento di forma, passivazione, DES, IL

Acknowledgements

I acknowledge the contribution of Alessandro Alleva, Benedetto Bozzini, Elisa Emanuele, Andrea Macrelli, Elie Paillard and Jiajia Wan to the investigation described in this study. If the research described in this thesis will be published as a journal paper, I plan to include an appropriate selection of these scientists in the co-author list, according to their relative input to the text that will be submitted.